DISCLAIMER:

This document does not meet the
current format guidelines of
the Graduate School at
The University of Texas at Austin.

It has been published for
informational use only.

The Dissertation Committee for Boum Hee Lee
certifies that this is the approved version of the following dissertation:

Algorithm-Aided Decision-Making in Reservoir Management

Committee:

Larry W. Lake, Supervisor

David A. DiCarlo

Robert B. Gilbert

Kishore K. Mohanty

Kamy Sepehrnoori

Algorithm-Aided Decision-Making in Reservoir Management

by

Boum Hee Lee

DISSERTATION

Presented to the Faculty of the Graduate School of

The University of Texas at Austin

in Partial Fulfillment

of the Requirements

for the Degree of

DOCTOR OF PHILOSOPHY

THE UNIVERSITY OF TEXAS AT AUSTIN

May 2019

To my parents.

Acknowledgments

Throughout my graduate studies, I have had the pleasure and privilege of working with Dr. Larry Lake. From Dr. Lake I learned the intellectual humility and honesty in acknowledging my ignorance, and the authenticity that follows when it is overcome. He also taught me by demonstration ways to cultivate and safeguard a sense of curiosity. I express my deepest appreciation for his patience and guidance. Thank you for always making it about the questions, and for allowing me the freedom to explore.

I am grateful to Dr. Robert Gilbert for kindling my interest in decision analysis, and for entrusting me with valuable teaching opportunities, from which I learned immensely. I cherish the experience, which I will be without were it not for Dr. Gilbert. I am also grateful for his NSF grant that allowed me to continue my studies.

I would like to thank Dr. David DiCarlo, Dr. Kamy Sepehrnoori and Dr. Kishore Mohanty for their valuable technical feedback on my dissertation. The discussions were a great pleasure on my part, knowing how rare it is to have experts with deep and diverse technical backgrounds take the time to review and share honest feedback on my work. Thank you.

My life in Austin has been blessed with friends who have always been supportive and inspiring. Here I shall attempt to thank at least some of them.

I am deeply appreciative of my previous and current office mates with whom I feel lucky to have shared the grad student experience: Nuntha Naudomsup, Yun Wu, Sean Pan, Bo Ren, Mahmood Shakiba, Azor Nwachukwu, Arin Raina, and Jose Salazar. Thank you for all the pleasant times full of jokes and interesting discussions. My special thanks to Behzad Eftekhari, whose clarity in reasoning helped me find my own. I will miss our debates and discussions that continued for hours on end.

I extend my thanks to many friends outside of my office: Brandon Tang, Ryan Leung, and Denning Wang for the great Graduate Bro experience, Philip Thomas and Aojie Hong for selflessly sharing their expertise on decision analysis and probabilistic methods, Hyunmin Kim, Bruno Fernandes, Olga Fuks and Karen Chen for the great internship experience, Kwanghoon Baek, Hunjoo Lee, Hoonyoung Jeong, Jongsu Hwang, and Hyungjoo Lee for the Korean PGE crew, and David Weaver and Roger Edmondson for sharing interesting projects and for inspiring in me a sense of usefulness. Also my thanks to Seunghwan Chun, Songhyun Baik, Jen Lee, Himanshu Sharma, and Yuseon Kim for your friendly support. Thank you all for the joyful memories.

Algorithm-Aided Decision-Making in Reservoir Management

Boum Hee Lee, Ph.D.
The University of Texas at Austin, 2019

Supervisor: Larry W. Lake

Sound reservoir management involves making decisions in the presence of uncertainty and complexity. Because projects handled in the oil and gas industry are often highly risky and uncertain, the decision-making methods the geoscientists employ must be self-consistent, systematic, and defensible.

This dissertation addressed three example problems commonly encountered in reservoir management: water injection allocation optimization, horizontal well refrac scheduling, and infill drilling scheduling. Solutions to each problem employ different algorithms and data analytic techniques that allow a coherent integration of uncertainty and decisions. The specific algorithms and statistical tools used for each problem are provided below.

The solution to water injection allocation draws from simple models as well as appropriate statistical methods. The capacitance-resistance model (CRM) is used to model interactions between injectors and producers to help

predict the reservoir's fluid production response. The CRM is paired with Koval's K-Factor method to decouple oil and water from total fluid production. The models are fitted using a bootstrapped dataset to generate a diverse distribution of history matched solutions. Next, the best injection scheme corresponding to each history matched model is determined using ensemble optimization (EnOpt). Finally, a sampling algorithm called Thompson sampling is called upon to determine the optimal injection scheme while reducing the number of less promising simulations. This way, one can select the best injection scheme that is robust to uncertainties in history matching while simultaneously minimizing the number of simulation runs where it is unnecessary. Validation against a reservoir simulation model is provided at the end to confirm that the injection scheme selected is indeed optimal.

The refrac scheduling problem examines a horizontal gas well that is a candidate to refracturing. The analysis employs a real options approach to find the current and future conditions in which refracing is the best decision, as well as to provide an accurate valuation that reflects the managerial flexibility of the project. An algorithm called least-squares Monte Carlo (LSM) will be used to achieve the two goals. In parallel, the Ornstein-Uhlenbeck model is calibrated using the ensemble Kalman filter (EnKF) to account for the gas price changes through time stochastically. The results of the valuations are compared against a myopic Monte Carlo/discounted cash flow (MC-DCF) method to demonstrate that the latter provides an underestimate of the true value. The underestimation results from that the MC-DCF approach neglects

the alternatives available in managing the project. The difference between the two estimates of project value is calculated to determine the value of flexibility. Finally, the optimal policies determined is examined to confirm that the recommended response to the realization of uncertainties is intuitively consistent.

Finally, a Monte Carlo tree search (MCTS) algorithm is paired with a reservoir simulator to optimize the infill drilling schedule in a reservoir undergoing waterflooding. Because of the permutative nature of sequence-dependent actions, the problem suffers from the curse of dimensionality. MCTS allows the user to find an approximate solution to the scheduling problem that is otherwise intractable. The final optimized schedule specifies 1) whether an infill well should be drilled at candidate locations, 2) whether an injector or producer should be drilled, and 3) when the well should be drilled. A provisional validation is provided at the end by comparing the cumulative oil production and the NPV of the MCTS-optimized schedule against those resulting from randomly generated schedules.

Overall, the goal of this dissertation is to demonstrate that different algorithms can be tailored to optimize decisions or policies. The proposed solutions systematically integrate the relevant uncertainties in the analysis as they search for the most preferred action. Such rational approach where uncertainty plays an active role in decision-making provides the geoscientists with the confidence that the final optimized decision is the best action to take. Workflows designed and recommended in this dissertation are strongly

preferred over the alternatives where uncertainty and sensitivity analyses are conducted after decisions have already been made using deterministic methods.

Table of Contents

List of Figures

Chapter 1

Introduction

In the oil and gas industry, engineers and geoscientists are challenged to make many different types of decisions. The decisions can vary in many ways, such as time-sensitivity, spatial-sensitivity, types of information relevant to the decision, and the uncertainties associated with the available information. Among many decisions that are commonly encountered in the industry, three example problems are selected and solved in this dissertation: water injection allocation optimization, horizontal well refrac scheduling, and infill drilling scheduling. The provided solutions to the problems will exemplify ways in which decisions and uncertainties are systematically integrated to logically and intuitively approach the optimal decisions.

In this dissertation, the three challenges will be analyzed in three fundamental ways. They will be investigated in terms of 1) the number of alternatives considered, 2) the time-sensitivity of the decisions, and 3) the extent to which the uncertainties are incorporated in the analyses. Suitable methods and algorithms will be proposed as solutions for each problem and will be applied to find optimal policies or decisions.

In solving the injection allocation problem in Chapter 2, we will pri-

marily focus on finding the optimal injection scheme while simultaneously managing the uncertainties associated with history matching. Because the number of alternatives in the possible injection schemes is infinite, the number of options considered is large. The proposed method actively combines this vast decision space with the uncertainty in history matching to find the injection scheme that is expected to yield the largest returns. In the way that the problem is formulated in this work, the impact of time-sensitivity is small.

The goal of Chapter 2 is to select the best injection scheme that is robust to uncertainties in history matching, while simultaneously minimizing the number of simulation runs where it is unnecessary. We will first take advantage of simple models to generate multiple alternatives of injection schemes we could implement to maximize oil recovery. Then an intelligent sampling method called Thompson sampling will be called upon to determine which one of the generated alternatives is likely to yield the most significant returns. Because a reservoir simulation model is considered to be the "true case" in this study, a validation is provided at the end of the chapter to illustrate that the final selected injection scheme is indeed optimal.

In the refrac schedule optimization problem of Chapter 3, the number of alternatives considered is small. The three available options are 1) maintain current production, 2) refracture the horizontal well, and 3) terminate production. Because the challenge is to find the optimal time of refracturing and termination, the problem is highly time-sensitive. The primary source of uncertainty considered for this study is the future gas prices.

The refrac scheduling challenge will be solved using the least-squares Monte Carlo (LSM) method. LSM is an algorithm designed for real options valuation of projects with a small number of available options. Two main advantages of using the LSM algorithm for this problem are 1) it provides an accurate valuation of the project that reflects its managerial flexibility, and 2) it outlines the optimal policy as a function of random variables included in the analysis. In other words, the LSM method incorporates the possibility of future refracing in its valuation and qualitatively informs us of current and future conditions in which refracing is the best decision. In this dissertation, we will apply the method to a horizontal gas well that is a candidate for refracturing. The results will then be analyzed to determine the value of flexibility, and examine how the optimal policy changes through time.

In the infill drilling scheduling section (Chapter 4), we will pair a reservoir simulation model with the Monte Carlo tree search (MCTS) algorithm to determine 1) whether an infill well should be drilled at different candidate locations, 2) whether an injector or a producer should be drilled, and 3) when the wells should be drilled. NPV will be used as a measure of schedules' optimality. Because the actions are sequence-dependent, the number of alternatives suffers from the curse of dimensionality, i.e. the number of alternatives are intractably large. Also, the order in which the wells are drilled has a significant impact on oil recovery, making the problem highly time-sensitive. Because the reservoir simulator used is relatively computationally costly, we assumed that the uncertainties associated with the models and reservoir's response to new

wells are deterministic. This shortcoming can be made up for by using simple models that have smaller computational costs, the potential alternatives of which is discussed in the Appendix section of the dissertation. A provisional validation is provided at the end by comparing the cumulative oil production and the NPV of the MCTS-optimized schedule against those resulting from randomly generated schedules.

Overall, the goal of this dissertation is to provide examples of how different algorithms can be tailored to optimizing decisions or policies. The proposed solutions systematically integrate the relevant uncertainties in the analysis while they search for the most preferred action. Such rational approach where uncertainty plays an active role in the decision-making process provides the geoscientists with the confidence that the final optimized decision is the best action to take. Workflows designed and recommended in this dissertation are strongly preferred over the alternatives where uncertainty and sensitivity analyses are conducted after decisions have already been made using deterministic models.

Chapter 2

Injection Allocation Optimization Using Thompson Sampling

2.1 Literature Review

Waterflooding is the use of water injection intended to increase pressure and displacement in the formation and consequently hydrocarbon recovery. In a reservoir that consists of injectors and producers, one of the key decisions involves determining how much water will be injected at each injection wells to maximize returns. The decision may be further complicated by limited injection water availability at different locations, by changing economic conditions, and by how water injection impacts the production differently at varying points in time and location, contingent on the static and dynamic conditions of the reservoir.

Many works have proposed solutions to this problem. For instance Liang et al. (2007) approached the problem using a combination of CRM, Gentil's (2005) two-phase model, and a simple cashflow model. CRM is used to account for total fluid production, Gentil's model to decouple oil and water rates from total fluid production, and the cashflow model to determine net present value (NPV). Liang et al. then put the combined model under a con-

strained nonlinear optimizer with a variety of economic conditions to observe how optimal injection schemes were affected.

Weber (2009) also studied the problem of injection allocation using CRM by deriving Kuhn-Tucker optimality condition for the NPV of the oil recovery problem. Kuhn-Tucker conditions are useful because if a given parameter set corresponds to a local minimum on the objective function, then it must satisfy the Kuhn-Tucker conditions. Therefore it can serve as an indicator that the optimized parameters are at local extrema. Using this configuration, Weber conducted sensitivity analysis on the economics of water flooding by varying oil price, water cost, and discount rate, and found that the NPV of predicted oil recovery behaves in a predictable manner.

Mandal et al. (2007) provided the solution a similar problem of allocating the injection water between reservoirs, rather than injection wells. The work solves the problem by calculating the individual water injection needs for every reservoir, and optimizing them by ranking key criteria. The factors that constitute the criteria for water injection needs include voidage replenishment ratio, threshold operating pressure above bubble point, conformance loss caused by injection out of pay, oil response per barrel of water injected, and crude quality. Mandal et al. then uses "influence functions" to determine weighting factors to each of the criteria, and uses the weighting factors and the criteria to find "rationalized injection allocation" that maximizes the value of injection water.

2.2 Models, Methods, and Algorithms Used

This section of the dissertation will list out the tools used to tackle the problem of injection allocation. The following section (2.3) will describe how these methods are woven together as the proposed solution to the problem. The models, methods, and algorithms to be described in the following sections are: the capacitance-resistance model, Koval's K-factor method, bootstrap analysis, and Thompson sampling.

2.2.1 Capacitance-Resistance Model (CRM)

Capacitance-Resistance Model (CRM) is a simple reservoir model that captures the relationship between injectors and producers in a reservoir undergoing waterflooding. It is designed to estimate the producers' liquid flow rates in response to varying liquid injection rates. There are multiple variants of CRM that define control volumes differently. CRM-Producer (CRMP) defines the control volume to be centered around producers and is the one selected for this research. The following equation describes the CRMP model.

$$\tau_j \frac{dq_j}{dt} + q_j(t) = \sum_{i=1}^{N_{inj}} f_{ij} w_i(t) - \tau_j J_j \frac{dp_{wf}^j}{dt} \tag{2.2.1}$$

$$\tau_j = \frac{c_t V_{p,j}}{J_j} \tag{2.2.2}$$

q_j: Liquid flow rate at producer j [bbl/mo]

w_i: Water injection rate at injector i [bbl/mo]

τ_j: Time constant for producer j [mo]

f_{ij}: Inter-well connectivity between injector i and producer j [frac.]

J_j: Productivity index for producer j [bbl/mo/psi]

p^j_{wf}: Flowing bottomhole pressure at producer j [psi]

c_t: Total compressibility [psi^{-1}]

$V_{p,j}$: Pore volume of control volume defined around producer j [bbl]

The model parameters of CRM can be categorized into three groups: the time constant (τ_j), the inter-well connectivity (f_{ij}), and the productivity index (J_j).

The time constant τ_j is a measure of the time necessary for the pressure wave (caused by a variation in the injection rate) to propagate in the porous media and effectively influence the production signal. The inter-well connectivity f_{ij} represents the volume fraction of injected water from an injector (i) that flows toward a producer (j), for each injector-producer pair at steady-state conditions (Sayarpour, 2008). The productivity index J_j is defined as flow normalized by the drawdown pressure, which serves as a measure of well potential.

If the reservoir is a closed system, and formation and fluids are assumed to be incompressible, the sum of inter-well connectivities should sum to unity.

If injected water is lost in the formation, the sum value is below one. If fluids other than injected water enter the control volume (for instance aquifer influx), then the sum value is larger than one. In this study, it is assumed that the sum of connectivities are less than or equal to one. The constraint was assigned through nonlinear optimizer implementation.

The flowing bottomhole pressure values are assumed to be determined operationally; they are accounted for in the history matching stage, but for making future projections and injection scheme optimizations, they are assumed to be constant. This is for us to clearly examine the oil production and net present value as functions of injection scheme, without flowing bottomhole pressures acting as confounding variables.

CRMP models total liquid rates; it does not differentiate between oil and water. To decouple oil and water production rates from total liquid production rates, I use the Koval model, which is presented in the next section.

2.2.2 Koval's K-Factor Method

It is well established that miscible displacements in the field can be unstable, depending on the mobility ratio. If unstable, the instability results in the solvent fingering through the oil, inducing early breakthrough and reducing sweep efficiency.

According to Koval (1963), instabilities in miscible displacements are attributed to four major factors: longitudinal dispersion, channeling, viscosity

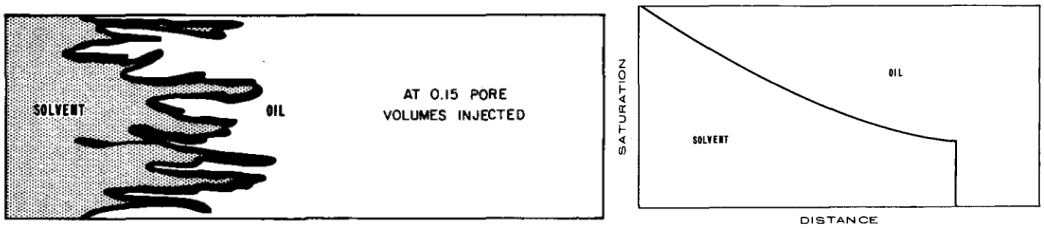

(a) Miscible Displacement Front

(b) K-Factor Method Modeling Solvent Saturation as a Function of Distance

Figure 2.1: Two-Dimensional Miscible Displacement Front and an Example Output of K-Factor Method (Koval, 1963)

differences, and gravity differences. To model for their impact on the emergence of fingering, Koval developed the K-Factor method. The schematic of the solvent fingering through oil and the K-Factor method's modeling of the phenomenon is provided in Figure 2.1.

The method introduces developments complementary to Buckley-Leverett's (1941) frontal advanced formula (2.2.3) and the fractional flow equation (2.2.4) to account for longitudinal dispersion, channeling, and viscosity differences. Koval controlled for the gravity effects by using matched density fluids in his experiments.

$$\left(\frac{\partial x}{\partial t}\right)_{S_{disp}} = \frac{q}{\phi A}\left(\frac{dF_{disp}}{dS_{disp}}\right) \tag{2.2.3}$$

$$F_{disp} = \frac{1}{1 + \frac{k_{oil}}{k_{disp}}\frac{\mu_{disp}}{\mu_{oil}}} \tag{2.2.4}$$

Re-writing the equation for solvent fractional flow in segregated flow using Koval's parameters (see Lake et al., 2014), we have the following:

$$F_S = \frac{1}{1 + \frac{1}{K_{val}}\left(\frac{1-S}{S}\right)} \tag{2.2.5}$$

K_{val} is the Koval factor, F_S is the solvent fractional flow, and S is the solvent saturation. The Koval factor is the product of a heterogeneity factor (H_k) and the effective viscosity ratio (E). The heterogeneity factor accounts for dispersion and channeling effects. Therefore K_{val} as defined below captures the aggregate effect of dispersion, channeling, and viscosity ratio on displacement front's stability in miscible flow.

$$K_{val} = H_k E \tag{2.2.6}$$

One way to estimate the effective viscosity ratio is to use an empirical relation (from Koval, 1963):

$$E = \left(0.78 + 0.22\left(\frac{\mu_o}{\mu_s}\right)^{\frac{1}{4}}\right)^4 \tag{2.2.7}$$

where μ_o and μ_s are oil and solvent viscosities, respectively. According to the above equation, the numerical value of effective viscosity ratio is smaller than that of the original viscosity ratio. This agrees with the observation that the effect of fingering caused by high viscosity ratio is not as prominent as it seems from the original viscosity ratio (Lake et al., 2014).

According to Lake et al. (2014), if we assume that relative permeability of oil and water are straight lines, the Buckley-Leverett equation can be integrated analytically to yield the following:

$$F_S|_{x_D=1} = \begin{cases} 0 & t_d < \frac{1}{K_{val}} \\ \frac{K_{val} - \sqrt{\frac{K_{val}}{t_d}}}{K_{val}-1} & \frac{1}{K_{val}} < t_d < K_{val} \\ 1 & t_d > K_{val} \end{cases} \tag{2.2.8}$$

$$t_{d,j} = \frac{W_j}{V_{p,j}} \tag{2.2.9}$$

where $F_S|_{x_D=1}$ is the fractional flow of solvent at the outlet ($x_D = 1$), t_d is dimensionless time, and K_{val} is the Koval factor, as described previously. The dimensionless time is defined by cumulative injected solvent (W_j), which is calculated using the CRMP model, and normalized by pore volume, (V_p).

In this study, equations (2.2.8) and (2.2.9) are used to decouple oil and water production rates from total fluid production rates. The parameters to be history matched are K_{val} and V_p, specified at control volumes defined around each producing well. This implementation is to ensure that the control volumes defined by CRMP are consistent with those used by the K-Factor method. The cumulative injected water (W_j) is also defined according to CRMP's definition of control volumes. History matching for Koval model's parameter is conducted simultaneously with the CRMP parameters using the ensemble optimization algorithm described in section 2.2.4. The Koval factor K_{val} for each control volume is treated as a parameter of its own, without separating the heterogeneity factor and the effective viscosity ratio.

2.2.3 Bootstrap

The bootstrap is a versatile statistical tool that is used to "quantify the uncertainty associated with a given estimator or a statistical learning method." (Friedman et al., 2009). It uses a resampling method on a set of observed data points to simulate and generate realizations of a statistic of the population distribution. The bootstrap is robust because it assumes non-informative prior; it does not require *a priori* information of the system nor the underlying probability distributions for the model parameters. However, for accurate results, it requires that the data be independently and identically distributed (i.i.d.) (Efron, 1977).

The bootstrap method works as follows. It randomly draws datasets with replacement from the observation data, each sample of the same size as that of the original observation dataset. This is done multiple times until a specified number of resampled sets are generated. Then the model is fit to each resampled set to produce a distribution of fitted model parameters. The distribution generated can be used to infer statistics of the model's parameters (Friedman et al., 2009). The resampling method generates multiple realizations that are perturbed versions of the original data, the statistics of which becomes an approximation of the Bayesian posterior (Friedman et al., 2009).

The primary form of the datasets used in this study is time series data. When the data has time dependence, then it is no longer likely to be independently and identically distributed because the data points often exhibit autocorrelation (Thomas and Lake, 2017). Carlstein (1985) proposed

the non-overlapping block bootstrap, which addresses this issue by dividing the time series into segments of equal lengths, and conducting sampling with replacement within every block to generate multiple instances of bootstrapped sample set. The blocked bootstrapping procedure proposed by Carlstein is visualized in Figure 2.2.

First, the original dataset is separated into blocks of equal lengths, as shown on the left side of the figure by orange vertical lines. Hall et al. (1995) has proposed a heuristic that guides the length of the blocks according to the total length of time series. $n^{1/3}$ is used as the block length, where n is the number of data points for a single time series. In the example in Figure 2.2, there are total of 18 data points, making the block length three data points.

After the block length have been determined, sampling with replacement is done within each block to generate multiple realizations, as visualized in the figures on the right column. The grey circles represent the possible values that each realization point could have taken. The possible values are determined by the value of data points within the block.

When a specified number of realization has been generated, a statistic is estimated for each realization. A statistic is then estimated using each bootstrapped realization is collected to generate distributions, which reflect the *a posteriori* uncertainty associated with estimation of those parameters.

The block bootstrap method is used in this study to generate a diverse set of history matched solutions that reflect the uncertainty in each

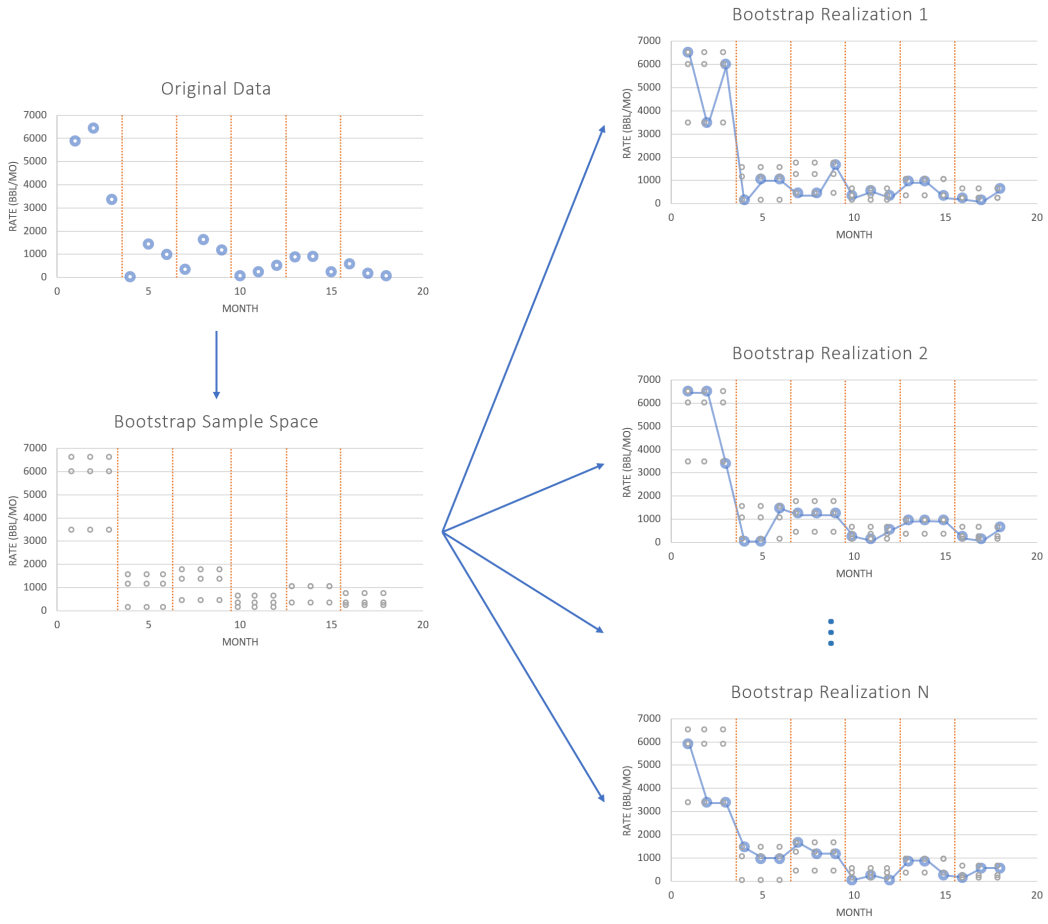

Figure 2.2: Block Bootstrapping Process Schematic

parameter. The advantages of the bootstrap method are: 1) that it does not require subjective input, including assignment of prior distributions, and 2) that the uncertainty resulting from applying the bootstrap method is easily reproducible. The details regarding the implementation is discussed in detail in the results section.

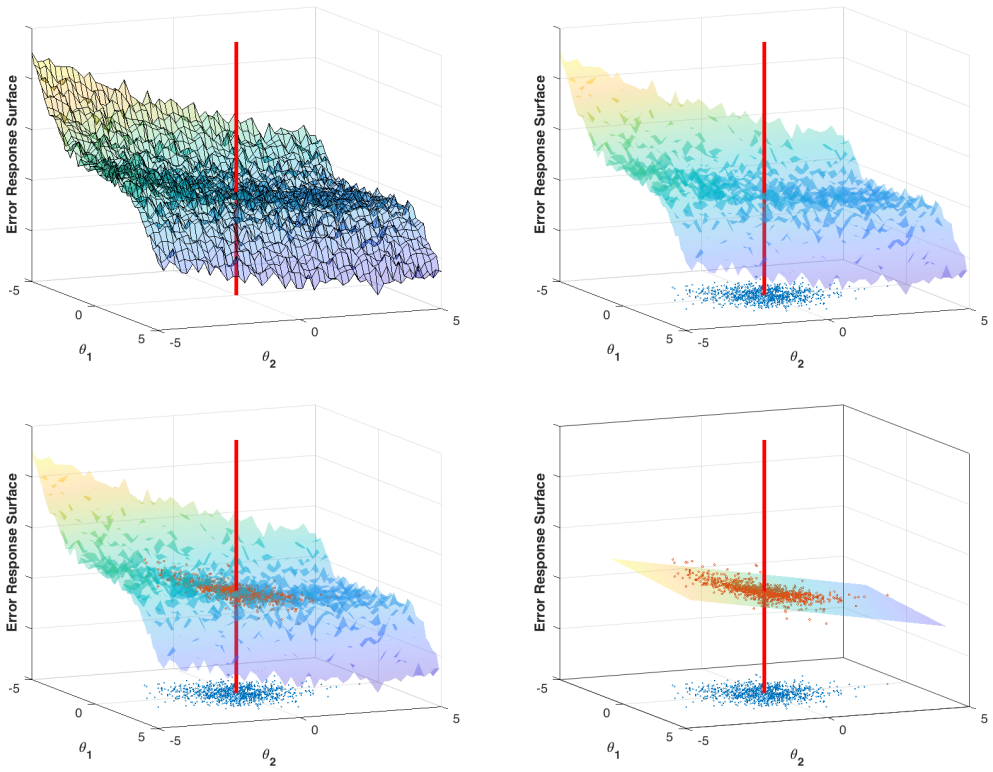

Figure 2.3: Stochastic Sampling to Approximate the Gradient at a Point on the Error Response Surface

2.2.4 Ensemble Optimization (EnOpt)

The ensemble optimization algorithm (EnOpt) is an optimization method based on the gradient-descent method. The discrepancy between EnOpt and the more traditional gradient-descent algorithms is that EnOpt estimates the gradients in the objective function space by a Monte Carlo sampling method. At every step of the optimizing iteration, the algorithm approximates the tangent plane at a point of interest in the parameter space by stochastic sampling, and the gradient in the corresponding objective function space is calculated

using the plane. The process of sampling in the parameter space (θ_i), and approximating the gradient at a point in parameter space is visualized in Figure 2.3. This approximation of gradient makes EnOpt robust to noisy local minima in the error function, and also renders the algorithm suitable for optimizing many parameters simultaneously. Other advantages of EnOpt include that it can significantly reduce the computational cost to determine the gradient, and that it can easily adapt to different types of functions (Hong et al., 2016).

Mathematical details regarding the EnOpt algorithm is provided as follows. The control vector is represented as a vector $\boldsymbol{x_i}$. This vector contains all the control variables (injection rates for every well and timestep) that will be modified by the algorithm to minimize the objective function $f(\boldsymbol{x})$.

$$\boldsymbol{x_i} = [x_1, x_2, x_3, \ldots, x_{N]i}^T \tag{2.2.10}$$

where $x_1, ..., x_N$ are the control variables to be adjusted by the algorithm, and N refers to the total number of control variables. The number of these individual control variables may be large, which prompts us to represent these variable in a vectorized form. The subscript $\boldsymbol{i}$ denotes the index for the ensemble member.

EnOpt uses an ensemble $\{\boldsymbol{x_1}, \boldsymbol{x_2}, \boldsymbol{x_3}, \ldots, \boldsymbol{x_i}, \ldots, \boldsymbol{x_M}\}$, which is sampled from a multivariate Gaussian distribution with specified distribution means $\bar{\boldsymbol{x}}$ and covariance matrix C_{xx}, representing the covariance between every

control variable. M denotes the total number of ensemble members. The $\bar{\boldsymbol{x}}$ value is updated iteratively as the optimization proceeds. For this study, the covariance matrix (C_{xx}) is kept constant. However, there are adaptive ways in which the covariance matrix is updated to achieve improved efficiency (Jansen and Fonseca, 2013), which is outside the scope of this dissertation.

The iterative updating of the control variable means ($\bar{\boldsymbol{x}}$) proceeds as described below. First, a mean-shifted ensemble matrix is computed for the control variables ($\boldsymbol{x}$) and the objective function values (f):

$$\Delta \boldsymbol{X} = [\boldsymbol{x_1} - \bar{\boldsymbol{x}}, \boldsymbol{x_2} - \bar{\boldsymbol{x}}, ..., \boldsymbol{x_M} - \bar{\boldsymbol{x}}]^T \tag{2.2.11}$$

$$\boldsymbol{f} = [f_1 - \bar{f}, f_2 - \bar{f}, ..., f_M - \bar{f}]^T \tag{2.2.12}$$

The $\bar{\boldsymbol{x}}$ and $\bar{f}$ are the mean values of control variables and the objective function values. $\bar{\boldsymbol{x}}$ is a component-wise mean of the control vector computed through all ensemble members, which results in a vector, while $\bar{f}$ is a scalar value. The calculations are done as below.

$$\bar{\boldsymbol{x}} = \frac{1}{M} \sum_{i=1}^{M} \boldsymbol{x_i} \tag{2.2.13}$$

$$\bar{f} = \frac{1}{M} \sum_{i=1}^{M} f_i \tag{2.2.14}$$

Once the mean-shifted ensemble matrix for the control variables ($\Delta \boldsymbol{X}$) and the objective function values ($\boldsymbol{f}$) are determined, then we estimate the gradient around the described by the vector $\bar{\boldsymbol{x}}$. The gradient is expressed as:

$$g = C_{xx}^{-1} C_{xf}, \text{ where}$$

$$C_{xx} = \frac{1}{M-1}((\boldsymbol{\Delta X})^{\boldsymbol{T}}(\boldsymbol{\Delta X})) \text{ and } C_{xf} = \frac{1}{M-1}((\boldsymbol{\Delta X})^{T}\boldsymbol{f})$$

The gradient calculated by the above equation can then be used to update the $\bar{\boldsymbol{x}}$ vector.

$$\bar{\boldsymbol{x}}^{l+1} = \bar{\boldsymbol{x}}^{l} + \alpha^{l} g^{l} \tag{2.2.15}$$

where l represents the iteration number, and α is the learning rate, which is a hyperparameter controlling for the tradeoff between stability and rate of convergence. In this study, the learning rate α is updated according to the following conditions:

$$\text{If } \bar{f}^{l+1} < \bar{f}^{l}, \text{ then } \alpha^{l+1} = \alpha^{l}/2$$

Iteratively updating to reduce the value of α incrementally slows the convergence rate while improving the stability.

In this study, the EnOpt algorithm outlined above will be used to determine the optimal injection scheme for each non-unique history matched

Figure 2.4: The Multi-Armed Bandit Problem

solution. The context and the results of its application will be discussed in the results section. For alternative discussion of EnOpt's algorithm and applications, the reader is recommended to review Chen and Zhang (2009).

2.2.5 Thompson Sampling

The multi-armed bandit problem has been extensively studied in statistics, operations research, computer science, and decision analysis literature. A bandit refers to a slot machine designed for the agent to pull a lever and observe the outcome on returns. The multi-armed bandit problem is summarized as follows: a slot machine has multiple levers, each lever associated with certain probability of success, or probability distribution of returns. The player has no knowledge of this probability. At every step in a sequence, the player has to decide which lever to pull to maximize the total returns. At the initial phase, the player ideally would experiment with different levers to estimate the probabilities of success for each lever, and as he gains a better estimate of these probabilities, eventually converge to pulling the lever that has the highest estimated probability of returns. As such, the multi-armed bandit problem

concisely exemplifies the tradeoff between exploration and exploitation that is commonly observed in machine learning problems.

Thompson sampling is one of many heuristics that guide the decision maker in navigating the exploration-exploitation tradeoff. It does so by referring to a prior distribution on the probability of returns associated with each decision, and by iteratively updating this distribution in a Bayesian framework to gradually resemble the actual probability of returns of the decisions with higher probability of large returns. It is interesting that the exploration is asymmetrical; the algorithm's exploration is preferential to the decisions that demonstrate higher returns. As the sequence progresses, the user converges to the decision that is close to the optimal decision. The algorithm is based on Thompson's foundational study investigating the issue of estimating probability with small number of observations (Thompson, 1983).

Figure 2.5 shows the process flow diagram for Thompson sampling. A brief description of each stage is provided in the following.

1. Specify identical initial distributions for outcomes associated with each decision (each handle of the slot machine).

2. For every decision (handle), simulate one realization of outcome using the outcome probability distribution. In other words, take one sample from the outcome distribution for each decision.

3. Pull the handle that resulted in the largest simulated return in step 2.

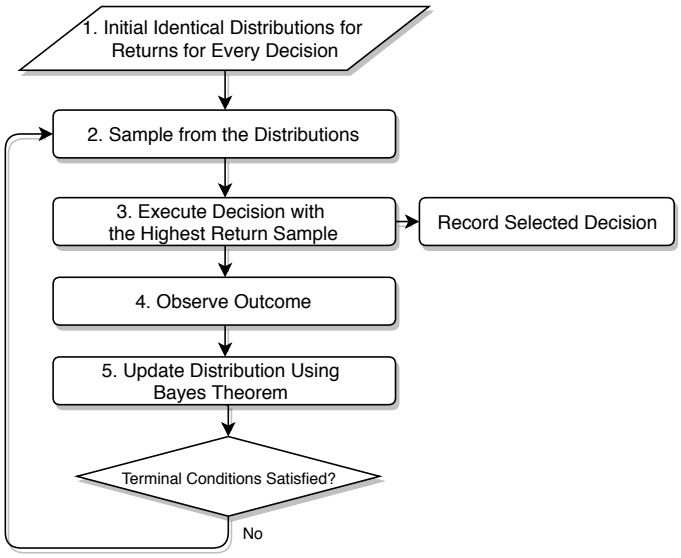

Figure 2.5: Process Flow Diagram for Thompson Sampling

4. Observe the outcome, and update the probability distribution for decision selected in step 3 using Bayes theorem.

5. Repeat until terminal conditions are satisfied. The posterior distribution becomes the prior in step 1.

When the algorithm has run sufficient iterations, it will tend to converge to repeatedly selecting the same decision. It is that decision that has the highest probability of maximum returns, as determined by the process.

In this study, Thompson sampling will be used to make educated guesses as to which injection scheme is the most likely to yield the highest returns given uncertainty in history matching, without having to try out every combination

of decision (injection scheme) and history matched model. This sampling method will allow the users to converge to near-optimal solution efficiently without having to exhaust all possibilities in the decision space.

A formal description of the algorithm is provided. Given a set of states $\mathcal{X}$, a set of actions $\mathcal{A}$, model parameters Θ, and rewards $\mathbb{R}$, the algorithm consists of the following:

1. A likelihood function $P(r|\theta, a, x)$
2. A set of Θ parameters θ of the distribution of r
3. A prior distribution $P(\theta)$ on these parameters
4. Past observation triplets $D = \{(x; a; r)\}$
5. A posterior distribution $P(\theta|D) \propto P(D|\theta)P(\theta)$, where $P(D|\theta)$ is the likelihood function

Thompson sampling consists of playing the action $a^* \in A$ according to the probability that it maximizes the expected reward, represented as follows:

$$\int \mathbb{I}\left[\mathbb{E}(r|a^*, x, \theta) = \max_{a'}(\mathbb{E}(r|a', x, \theta))\right] P(\theta|D)d\theta \tag{2.2.16}$$

where the $\mathbb{I}$ is the indicator function.

In practice, the rule is implemented by sampling, in each round, a parameter θ^* from the posterior $P(\theta|D)$, and choosing the action a^* that maximizes $E(r|\theta^*, a^*, x)$, i.e. the expected reward given the parameter, the action, and the current context. Conceptually, this means that the player instantiates their beliefs stochastically in each round, and then acts optimally according to them. In most practical applications, it is computationally onerous to maintain and sample from a posterior distribution over models. As such, Thompson sampling is often used in conjunction with appropriate sampling techniques.

For an alternative explanation and set of examples, the reader is encouraged to review Russo et al. (2017).

2.3 Experiment Formulation & Results

This section of the dissertation will walk the reader through the proposed workflow to find the optimal decision in the presence of uncertainty in history matching, as well as to correctly capture the uncertainty. The proposed workflow aims to reduce unnecessary computation by intelligently striking a balance between exploration and exploitation (as explained in section 2.2.5) in decision and model parameter space.

Figure 2.6 provides a visual overview of the process. In broad terms, the process is summarized in four steps: acquiring production history, generating multiple history matched solutions, determining the optimal injection scheme for each history matched model, and determining which one of the

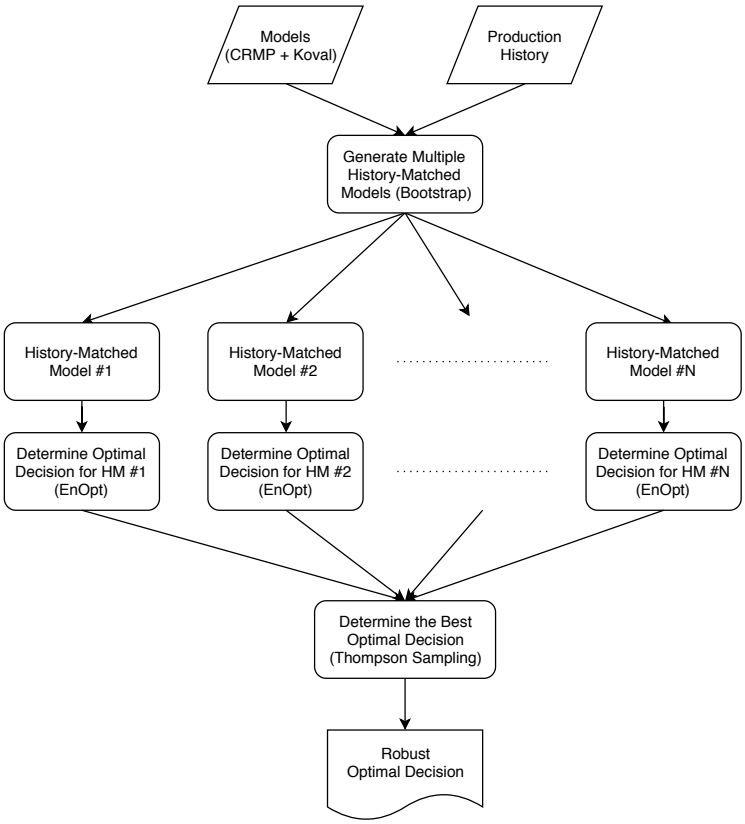

Figure 2.6: Workflow to Determine Optimal Injection Schemes Robust to Non-Uniqueness in History Matching

many decisions are likely to be truly optimal, in the presence of uncertainty. A validation of the final results will also be provided at the end. Each of these stages are discussed in detail in the sections that follow (2.3.1-2.4.2).

2.3.1 Obtain Production History

The first step is to obtain the production history of the reservoir. For field application of this procedure, the user will gather production data for

each well, including: injection rate history, water and oil production rates, and bottomhole pressures for producers (if available). For the purposes of the demonstration, I will generate these data from a commercial reservoir simulator. Using the simulation model as a base case is advantageous in validating that the method is robust, and is fit for field applications. The details of generating the production history for this experiment is detailed below.

I have used CMG commercial reservoir simulator to generate the data. A two-dimensional sector model is taken from the original SPE-10 model[1]. The wells are placed with an inverse five-spot pattern. The reservoir model has 13 total wells, consisting of four production wells and nine injection wells. A larger number of injectors than that of producers is chosen to increase the dimensionality of the decision space, which challenges the workflow and the algorithms used for the analysis.

A figure of the properties of the model is visualized in Figure 2.7. Using this reservoir model and an arbitrary injection scheme, a set of production data is generated. Figure 2.8 shows the injection scheme used to generate the historical production rates, and Figure 2.9 visualizes the flowing bottomhole pressure boundary conditions imposed on the production wells for simulation. Figure 2.10 summarizes the production response from the injection scheme.

The injection scheme was generated using simple random walkers. This is done by first selecting a rate value from a uniform distribution, and main-

[1]The model can be downloaded from https://www.spe.org/web/csp/datasets/set02.htm

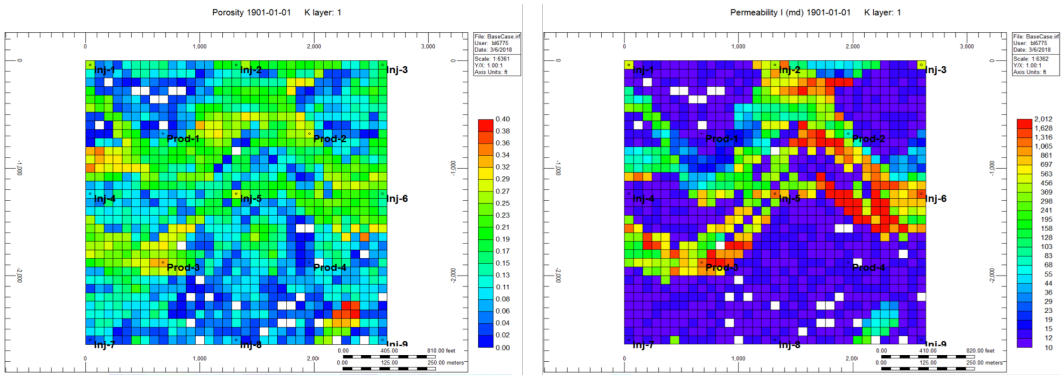

Figure 2.7: Porosity and Permeability Field of the Sector Model (from SPE-10)

taining that rate for a duration selected from another uniform distribution. Flowing bottomhole pressures for producers is another set of boundary conditions required for simulation, and are generated similarly (Figure 2.9). The uniform distribution from which the values are drawn are defined by minimum and maximum values, which were chosen so that the production rates are within reasonable bounds.

The generated injection rates (Figure 2.8) and producing bottomhole pressures (Figure 2.9) were provided as inputs to the simulator, which produced total fluid production rates and oil production rates (Figure 2.10).

The reservoir model will be used as a "true" case, against which the quality of decisions and forecasts will be compared. We will assume that the point at which the simulation ends is the present; any time period beyond this point will be considered future projections. Assuming the reservoir model is the "true" case has an important advantage in that it allows us to implement various decisions, the outcomes of which can be compared with simulation. If

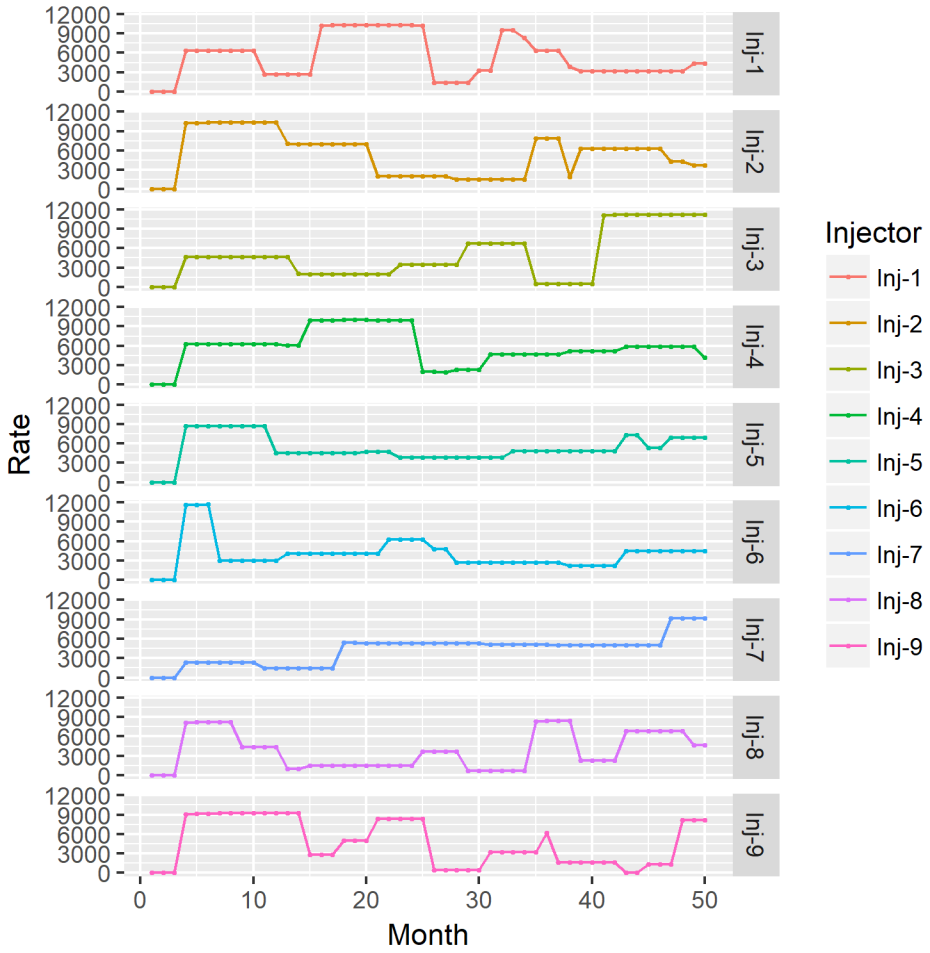

Figure 2.8: Injection Schemes Imposed on Injectors to Generate Historical Production Data (Rates in bbl/mo)

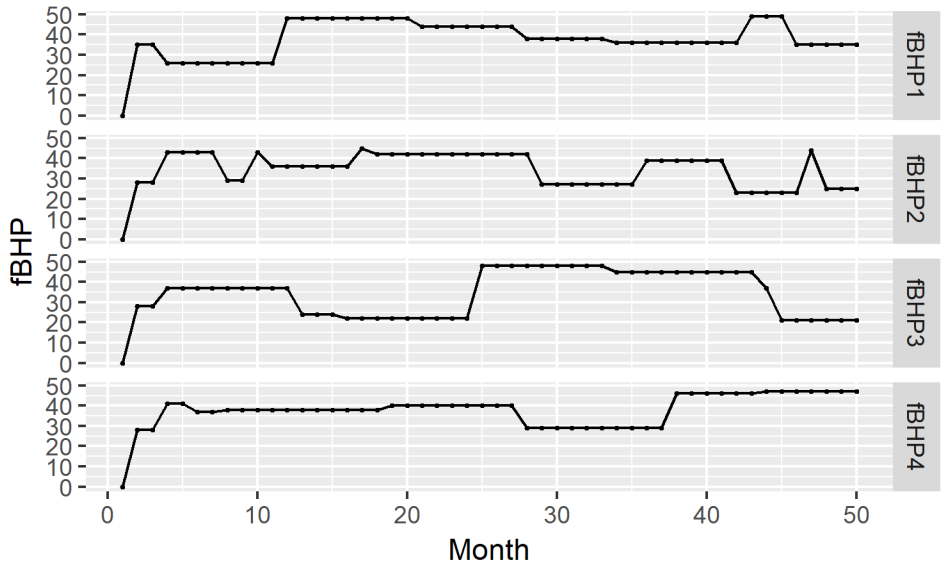

Figure 2.9: Flowing Bottomhole Pressure Boundary Conditions Imposed on Producers to Generate Historical Production Data (Pressures in psi)

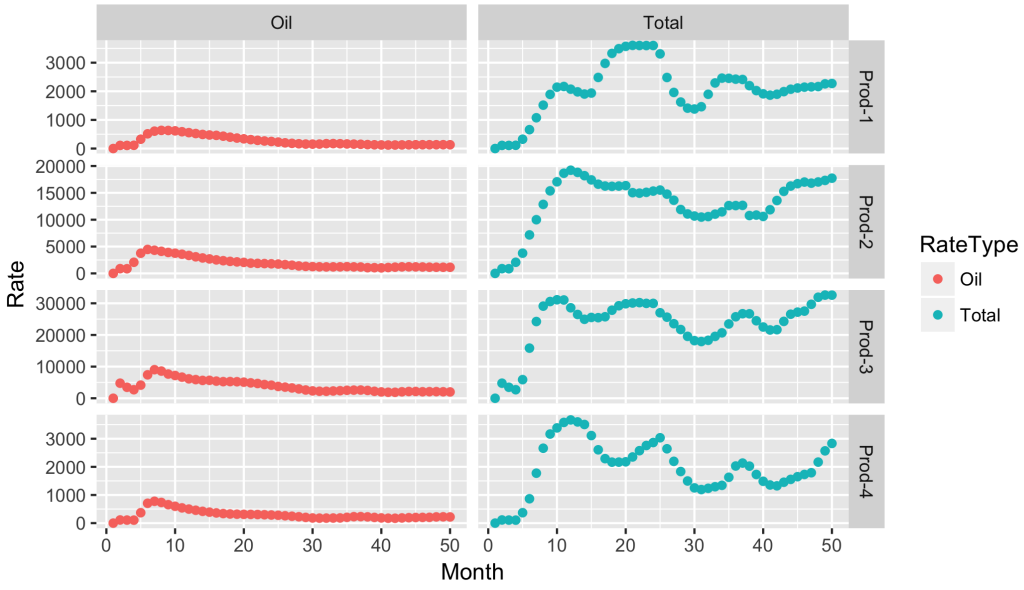

Figure 2.10: Total Fluid and Oil Production Responses (Rates in bbl/mo)

this method of analysis were to be used for field data, then it is advisable to consider the field data to be analogous to the simulation result data in this demonstration.

2.3.2 Generate Multiple History Matched Solutions

There is evidence that suggest that the best estimate of the model parameters do not coincide with the best estimate of the model's output (Tavassoli et al. 2004, Begg et al. 2004). Considering this, as well as that we fit model parameters to generate forecasts for different scenarios, we must take an alternative route. This method relies on the bootstrapping approach to unbiasedly capture the uncertainties around the model parameter estimation so that we can translate this uncertainty into subsequent analyses, including one that attempts to determine the optimal decision robust to the uncertainties.

Once the historical production data is acquired (as described in the previous section), then begins the history matching procedure. To produce an ensemble of history matched models consistently, I first generate multiple realizations of the original historical production data using the block bootstrapping method (a resampling method). The perturbed realizations of the original dataset is then used to fit the CRMP and Koval models using standard nonlinear regression techniques (MATLAB's `fmincon` functions).

200 bootstrap realizations were generated for this study, yielding 200 model parameter sets for both CRMP and Koval. The distributions of each parameters for both of these models are provided in Figures 2.11 and 2.12.

The well connectivity values in 2.11 are visualized in linear scale because the theoretical bounds of the values are 0 and 1. In 2.12, the productivity indices (J_i) are in units of bbl/mo/psi, time constants (τ_i) are in months, and the pore volumes ($\check{V}_p$) are in units of bbl; other parameters are dimensionless.

The uncertainty around the estimated model parameters can then be translated into uncertainties in the history matched models, represented as the fits to the original data points. The diverse set of fits are visualized in Figures 2.13 and 2.14.

The history matched model parameter sets as shown in Figures 2.11 and 2.12 represent the non-uniqueness and uncertainty in the models' history matching. In the next section, we will attempt to find the optimal decision that both maximizes the expected returns, and also is the most likely to be the best decision in the presence of uncertainty in history matching.

2.3.3 Determine Optimal Injection Schemes

So far, we have generated stochastically diverse history matched solutions that capture the uncertainty around the estimated model parameters. The next step is to determine the optimal decision designed for every history matched solution. Note that this is possible only when employing a simple model with a very small computational cost, as is the case with CRMP-Koval model combination.

Optimal injection will be determined using the ensemble optimization

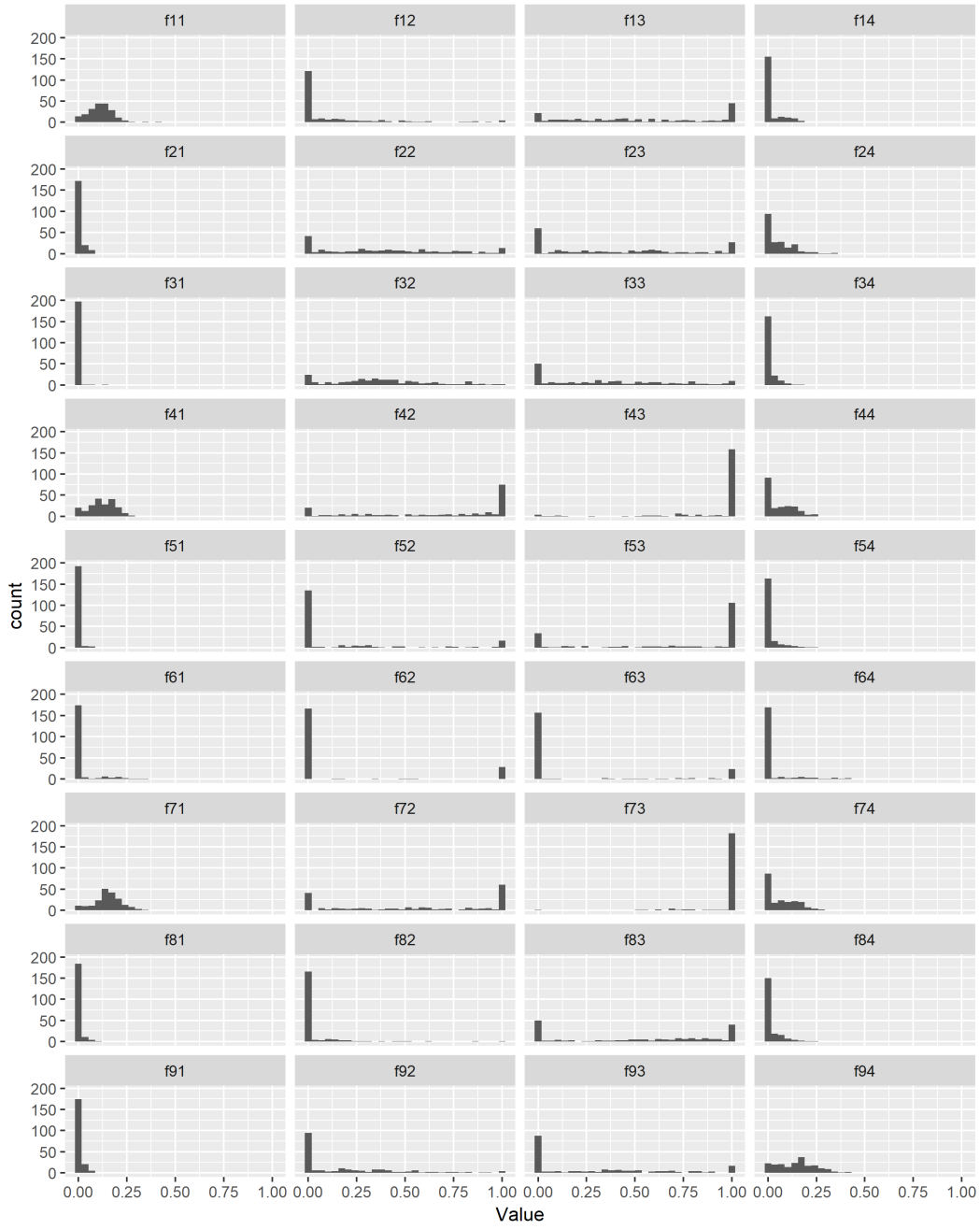

Figure 2.11: Histogram of Fitted Model Parameters for CRMP Connectivity Values

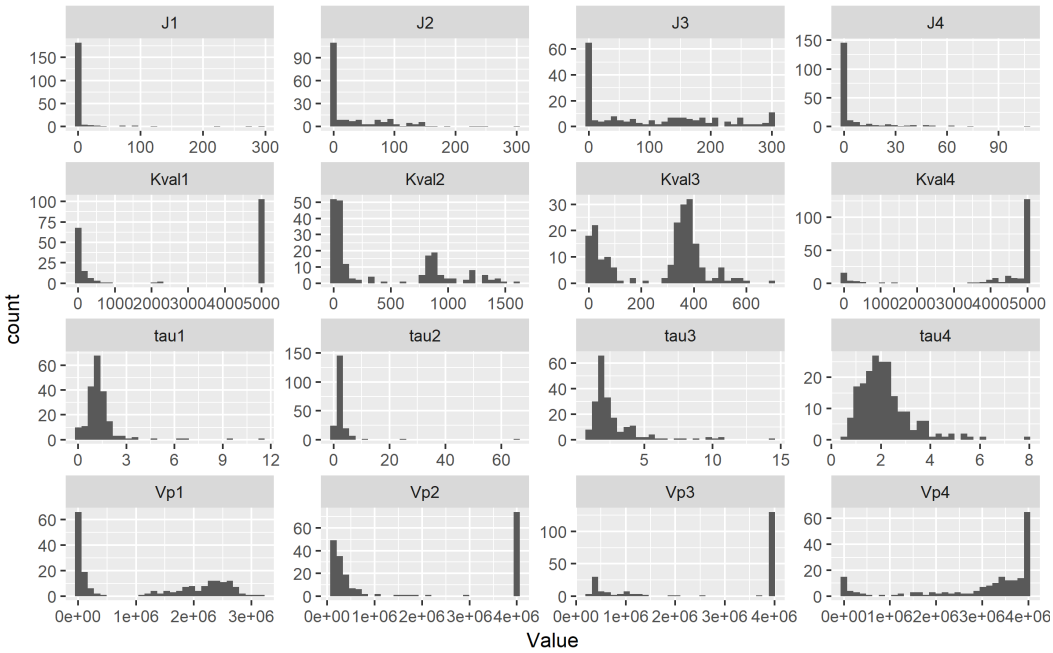

Figure 2.12: Histogram of Fitted Model Parameters for CRMP and Koval

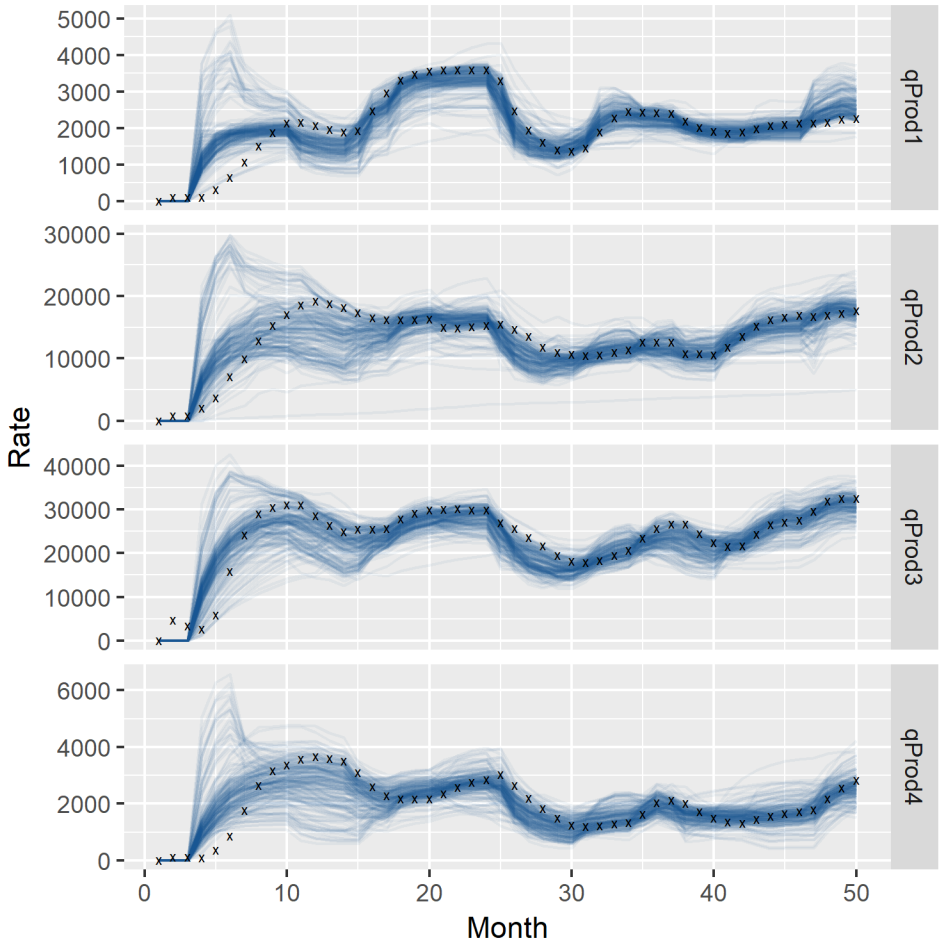

Figure 2.13: Simulator-Generated Total Fluid Production Data (Black Crosses) and CRMP Fits of 200 Bootstrapped Models (Blue Lines) (Rates in bbl/mo)

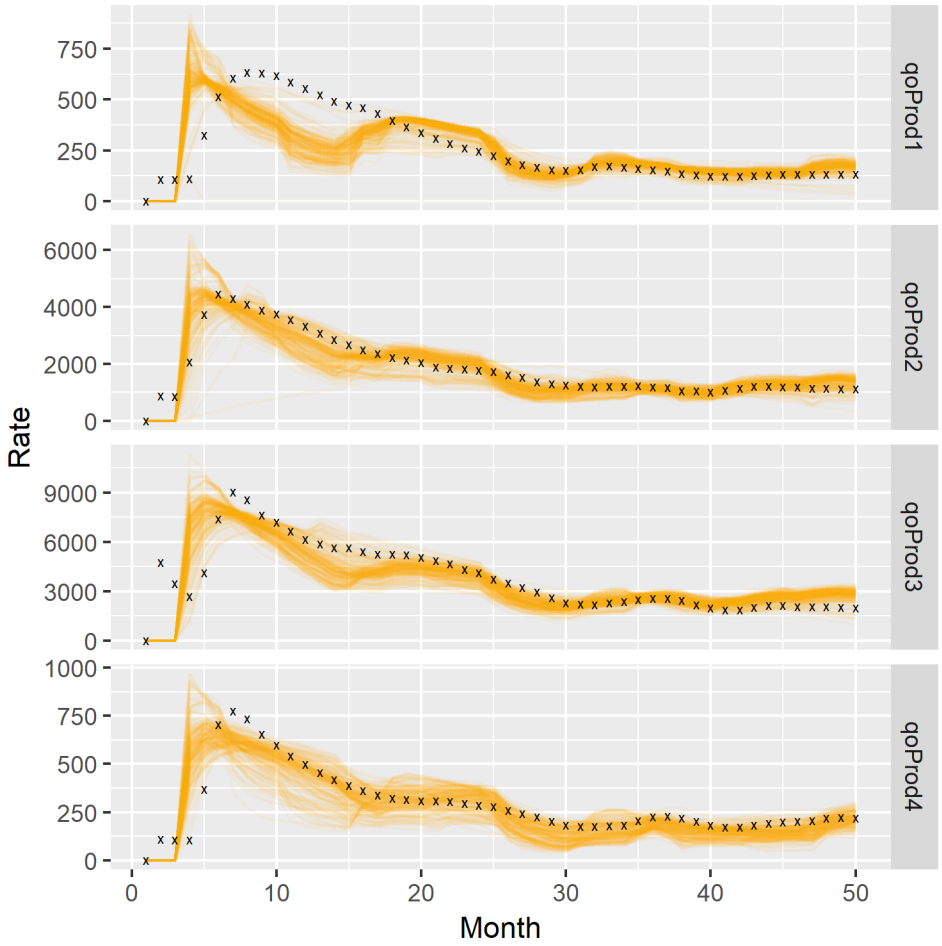

Figure 2.14: Simulator-Generated Oil Production Data (Black Crosses) and CRMP-Koval Fits of 200 Bootstrapped Models (Yellow Lines) (Rates in bbl/mo)

Factor	Value	Unit
Oil Price	60	$/bbl
Water Injection Cost	1	$/bbl
Produced Water Treatment Cost	0.1	$/bbl
Discount Rate	0	%
Local Injection Rate Lower Constraint	0	bbl/mo/well
Local Injection Rate Upper Constraint	14000	bbl/mo/well
Fixed Flowing Bottomhole Pressure (Producer)	50	psi
Schedule Optimization Duration	50	mo.

Table 2.1: Economic and Operational Constraints Used for Injection Scheme Optimization

(EnOpt) algorithm, the details of which is provided in section 2.2.4. The economic and operational constraints applied to these optimizations are in Table 2.1.

The discount rate selected to calculate the NPV is set to zero because, depending on how aggressively the discounting factor is set, the EnOpt algorithm gradually diminishes the future operations' contribution to the NPV while optimizing. Because of this, the injection rates the EnOpt optimizes quickly trails off to zero. As one may expect, the profiles with which the injection rates drop are strongly dependent on the discount rate. To eliminate the need to justify a specific value of the discount rate, the optimization constraint is set so that the cumulative net revenue over the 50 month interval is maximized. Figure 2.15 shows the optimized injection rates for the nine injectors for all 200 history matched CRMP & Koval models. The injection scheme tails off towards the end of the 50-month period because as we approach the end of the optimization time interval, the returns from injection will be observed

beyond the optimization interval. The rate at which it tails off is partly dependent on how quickly the producers respond to the injection rates, which is represented by the parameter τ_j in the CRMP model. In Figure 2.15, the colors indicate the optimal injection schemes corresponding to different history matched solutions.

We have determined the best injection scheme for every history matched model. In the following section, we will determine which one of these decisions should be actually implemented.

2.3.4 Determine the Final Injection Scheme

At this stage, we now have multiple non-unique history matched models, and the optimal injection scheme that maximizes the estimated NPV for every corresponding history matched model. The question that this section of the dissertation attempts to address is: given the uncertainty in the history matched models, which injection scheme should we choose to implement in real life? In other words, the challenge is to find the "optimal of optimals."

We have 200 history matched models representing the uncertainty associated with our model in relation to the true reservoir, and also 200 possible alternatives that we have determined given each history matched model is true. A brute-force way of determining the optimal choice would be to try out every injection scheme in all 200 history matched models, calculate the economics, and select the injection scheme that yields the largest expected returns. However, this is computationally inefficient as it requires a total of

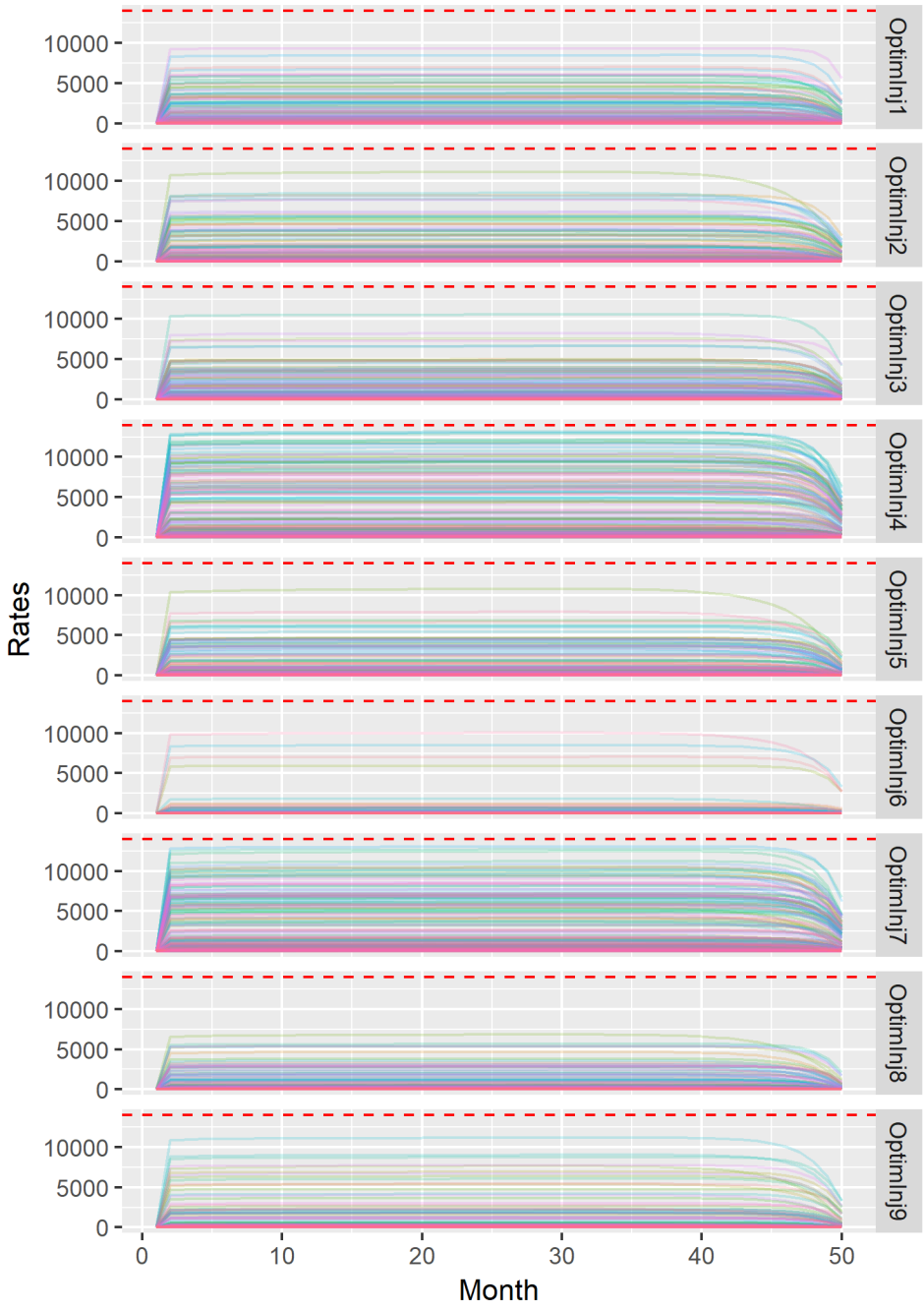

Figure 2.15: Injection Scheme Optimized for Each History Matched Model Using EnOpt (Rates in bbl/mo)

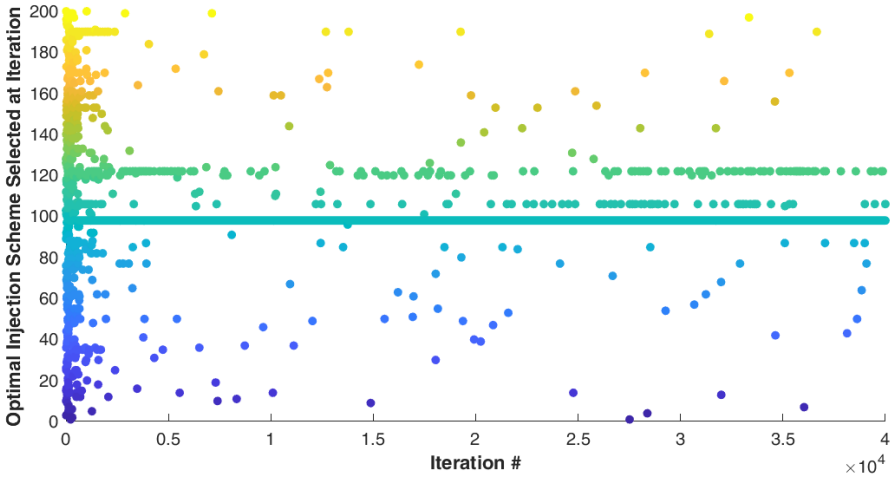

Figure 2.16: Plot of Selected Injection Schemes Through Thompson Sampling Iterations

40000 simulations. Thompson sampling will help answer the question, which will lead us to the final recommendation for water injection scheme.

Figure 2.16 shows which of the injection schemes were selected at every iteration step during the Thompson sampling process. In the beginning, the Thompson sampling algorithm does a breadth-first search through the decision space, and, after a certain amount of data has been collected, it transitions to best-first search. The indices of the top three most frequently selected injection schemes are 98, 122, and 105. Even when the updated distributions (the final iteration of which is shown in Figure 2.17) tell us that these decisions are the most likely the best, it also occasionally explores other decisions to increase confidence that the optimal is truly the optimal.

Figure 2.16 shows the number of searches (number of points along the

Rank	Inj. Scheme Index	Count	Rank	Inj. Scheme Index	Count
1	98	38814	...	...	...
2	122	219	171	156	2
3	105	160	172	157	2
4	190	43	173	158	2
5	88	21	174	162	2
6	133	20	175	163	2
7	82	19	176	165	2
8	62	14	177	167	2
9	85	14	178	168	2
10	197	14	179	171	2
11	39	13	180	173	2
12	124	12	181	174	2
13	35	11	182	176	2
14	87	11	183	177	2
15	138	11	184	178	2
16	12	10	185	179	2
17	18	10	186	180	2
18	77	10	187	181	2
19	161	10	188	183	2
20	36	9	189	185	2
21	50	9	190	187	2
22	131	9	191	188	2
23	143	9	192	191	2
24	55	8	193	192	2
25	128	8	194	193	2
26	14	7	195	194	2
27	30	7	196	195	2
28	54	7	197	196	2
29	59	7	198	198	2
30	66	7	199	17	1
...	...	...	200	103	1

Table 2.2: Number of Times an Injection Scheme was Selected by the Thompson Sampling Algorithm, Ranked (Top & Bottom 30)

x-axis) was set to the number of searches required to do a complete search, i.e. simulating for every possible combination of history matched model and the injection scheme (200 history matched models, and 200 optimal injection schemes for each model). That the Thompson sampling algorithm manages to converge to a few optimal injection schemes well before it reaches the number of simulations required to exhaust the model-decision space attests to the value of this method.

Table 2.2 shows the number of times each injection schemes were sampled by the Thompson sampling algorithm, sorted (the list shows the top and bottom 30). A quick inspection of the full table reveals that the Thompson sampling algorithm evaluates all of the injection schemes at least once.

Figure 2.17 visualizes the updated distributions of NPVs for each decision (injection scheme) after the final Thompson sampling iteration. The figure shows that the injection schemes with the higher expected NPVs tend to have lower uncertainty (standard deviation around the mean), because it has undergone more frequent preferential sampling, which has resulted in increased confidence in expected returns. The injection scheme indices for the top three highest peaks correspond to the top three most frequently selected in Figure 2.16.

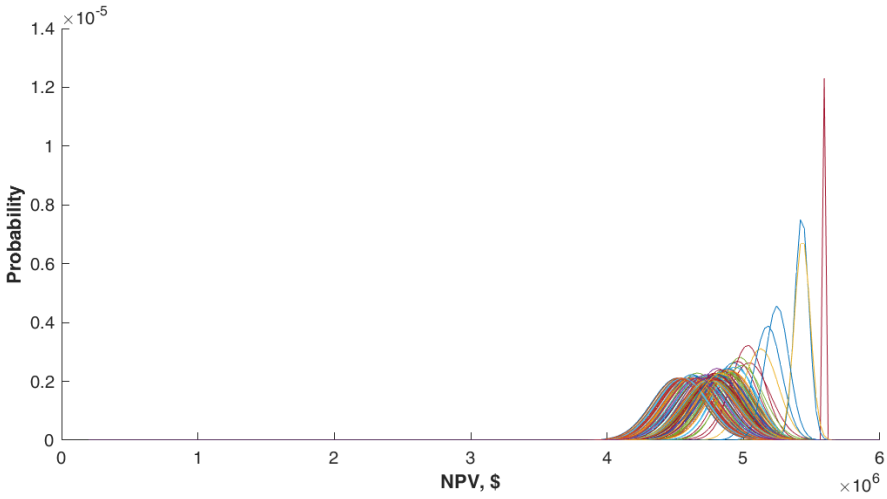

Figure 2.17: Estimated NPV Distributions for Each Decision After the Final Thompson Sampling Iteration

2.4 Results Validation

This section of the dissertation proposes a method to validate the outcome from section 2.3, and provides the results of validation.

2.4.1 Validation Method

The method used to validate the results from the previous section is simple. The CMG simulator will simulate the results of all 200 "optimal" injection schemes determined from 200 different history matched solutions, and calculate the net returns from each reservoir response. The results from CMG simulations will then be compared with the injection schemes that were selected at the top of the list after processing using the Thompson sampling.

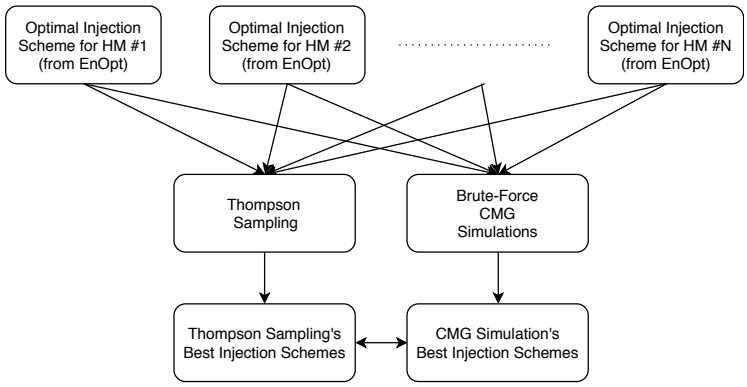

Figure 2.18: Validation Process Diagram

Because the Thompson sampling's behavior eventually converges to that of a best-first search algorithm, only the highest-ranked injection schemes will be compared from the two lists. The experimental design proposed above for history matching the models and determining the optimal injection schemes are summarized as a process flow diagram below in Figure 2.18.

2.4.2 Validation Results

So far, the Thompson sampling has determined a number of injection schemes to be optimal, i.e. robust to the uncertainties associated with history matching, and expected to yield highest returns. This section will verify that this is true by exhaustively subjecting the numerical reservoir model (in CMG) to every injection schemes found in section 2.3.3. In other words, all 200 injection schemes from section 2.3.3 will be used as input to the CMG simulator, and the results will be collected. Then we will examine how the

Rank	OptimInjScheme	qoProdCum	Rank	OptimInjScheme	qoProdCum
1	98	416606.5	...	...	...
2	88	413484.9	181	83	353156.7
3	153	408830.6	182	17	353102.2
4	106	406950.4	183	110	353085.5
5	62	406852.2	184	43	353032.4
6	55	406817.4	185	192	353003.7
7	190	402993.6	186	162	352949.9
8	99	402573.6	187	183	352829.8
9	59	402082.2	188	135	352792
10	37	400417.2	189	103	352760
11	54	400346	190	129	352706
12	120	400024.5	191	196	352698.9
13	150	399935.9	192	34	352690.9
14	77	399824.3	193	8	352684.2
15	82	399485.7	194	19	352656.8
16	122	398932.2	195	145	352644
17	105	398437.1	196	79	352639.1
18	35	398153.5	197	163	352637.3
19	159	397695.9	198	180	352609.6
20	87	397333.1	199	56	352576.7
...	...	...	200	193	352573.6

Table 2.3: Injection Schemes' Performance in CMG Simulation (in Cumulative Oil Production)

top few injection schemes selected from Thompson sampling fares in the list of actual performance results derived from the simulation.

Figures 2.19-2.21 visualize different rate responses generated from the simulations. Figures 2.19 and 2.20 show the total fluid (oil and water) and oil production rates at a per-well basis, while Figure 2.21 shows the cumulative oil production. All three figures visually represent the variability in results depending on which optimized injection scheme we choose.

Table 2.3 shows the CMG simulator's response to every injection scheme, numerically represented in terms of cumulative oil production. Comparing the

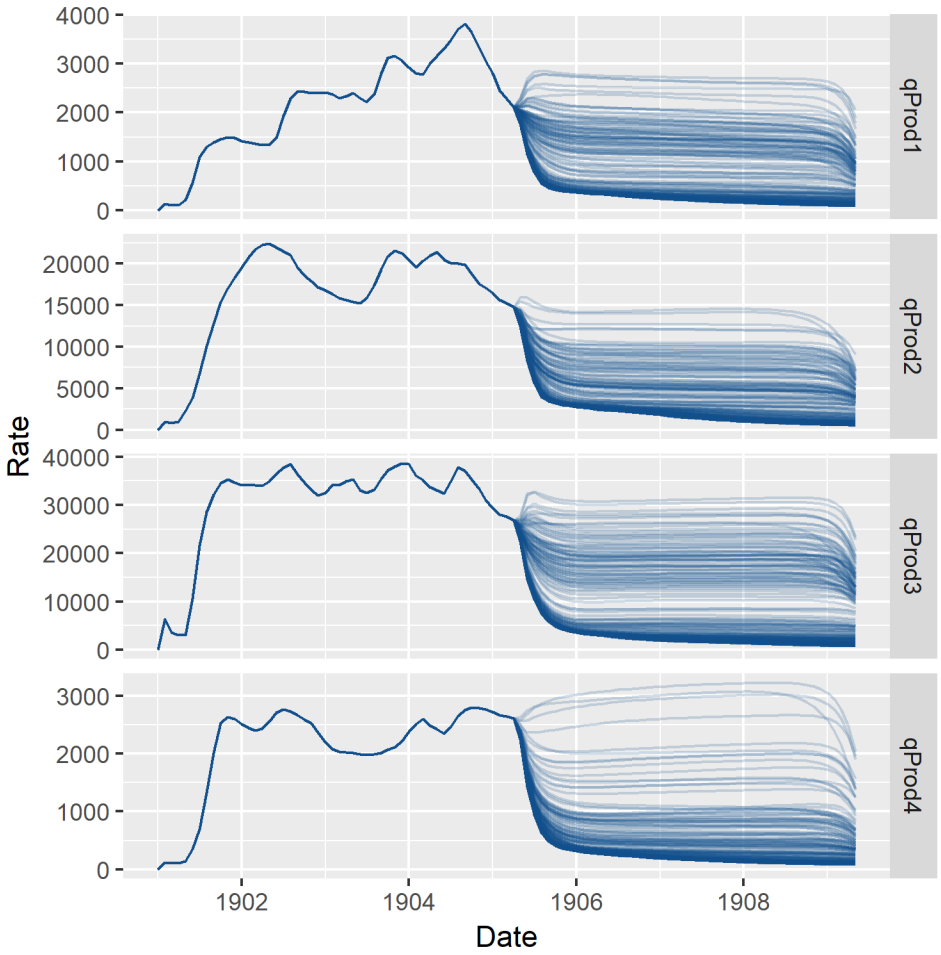

Figure 2.19: Total Fluid Production Rates: CMG Response to Every Optimized Injection Rate (bbl/mo)

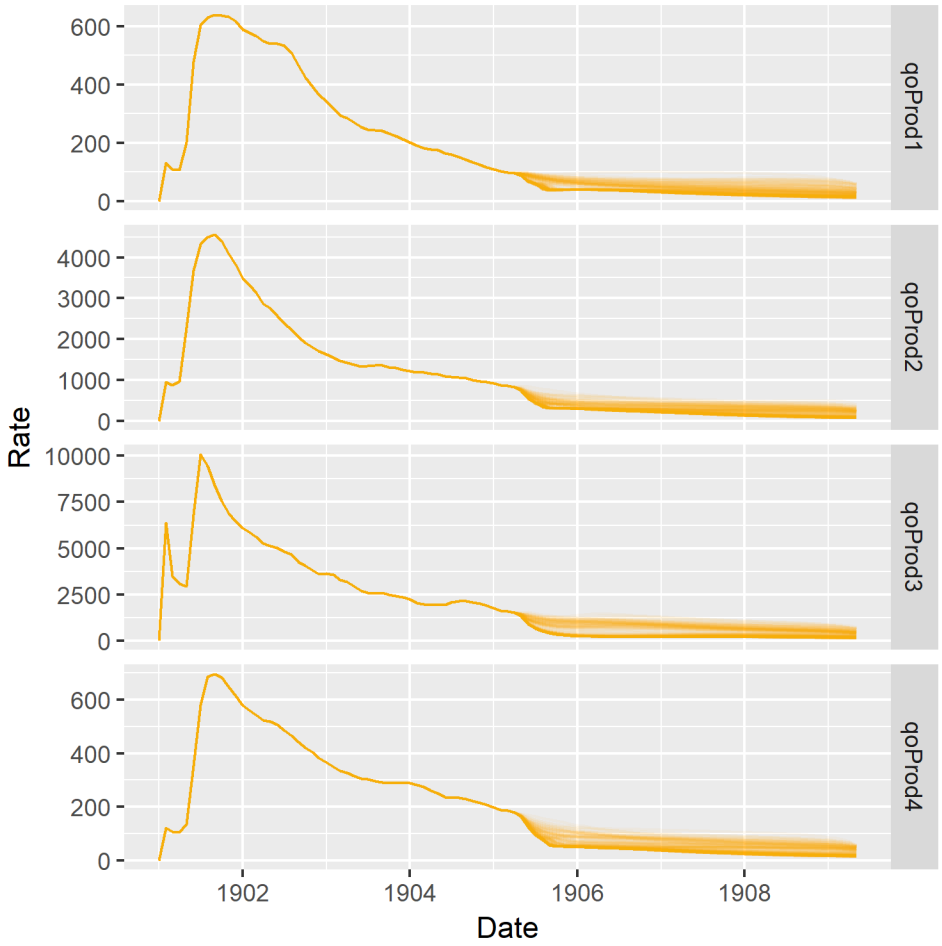

Figure 2.20: Oil Production Rates: CMG Response to Every Optimized Injection Rate (bbl/mo)

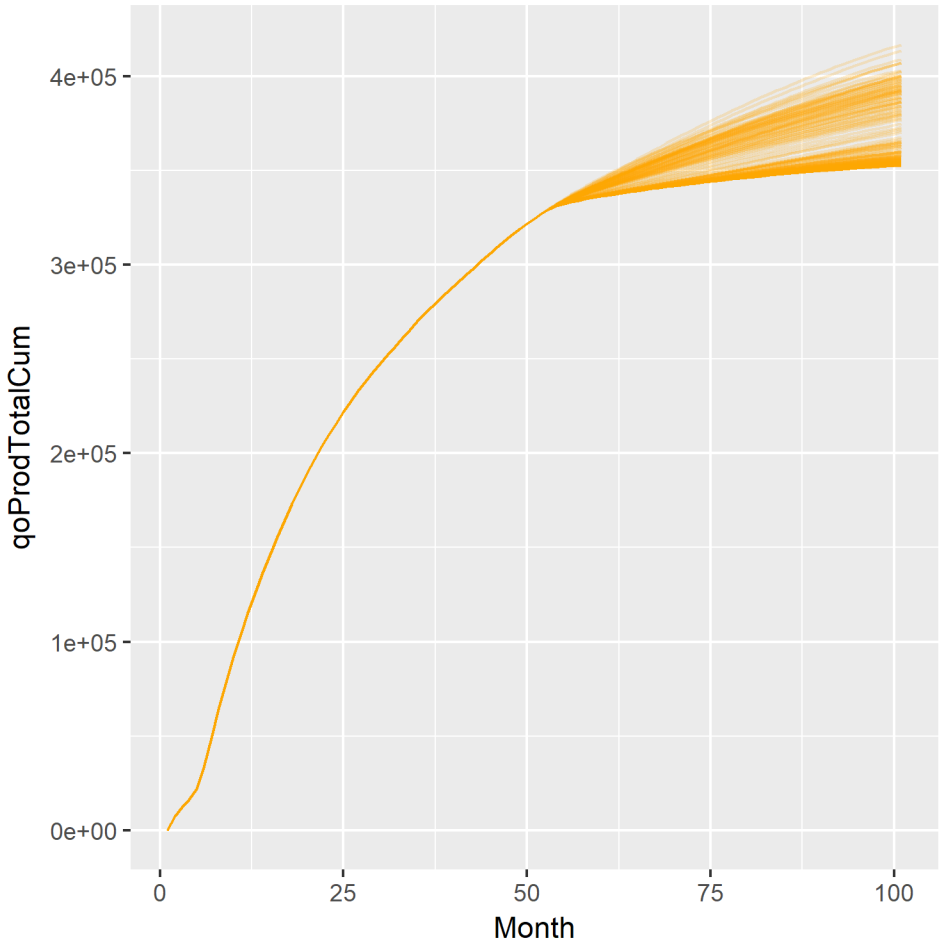

Figure 2.21: Oil Production (Field Cumulative): CMG Response to Every Optimized Injection Rate (bbl)

simulation results in Table 2.3 with the number of times the decisions have been selected by Thompson sampling algorithm (Table 2.2), we can see that the top index for injection scheme coincides. It is promising that the two indices match, because it indicates that the Thompson sampling successfully shifted through the uncertainty in history matching to determine the optimal injection scheme.

The final comparison is provided by computing the NPVs for each injection/production scenario. The histogram in Figure 2.22 visualizes the NPV resulting from running each injection scheme. The green dotted vertical line indicates the NPV achieved by the injection scheme selected using the Thompson sampling method, as outlined in this chapter. To demonstrate the advantage of this method, this value is compared against a base case, as denoted by the red dotted vertical line in the figure. The NPV value for the "Deterministic" is the NPV that results from taking the injection/production history (from CMG simulation), fitting the CRM+Koval model, and optimizing the injection scheme using ensemble optimization (EnOpt) algorithm. The larger NPV value resulting from Thompson sampling demonstrates that it was able to find a more optimal injection scheme that bypasses the local maximum NPV of a single deterministic case. Although the probabilistic method required a larger number of simulation runs to achieve this result, the lightness of simple models paired with Thompson sampling to further reduce unnecessary simulations placed this method well within reasonable computational limits.

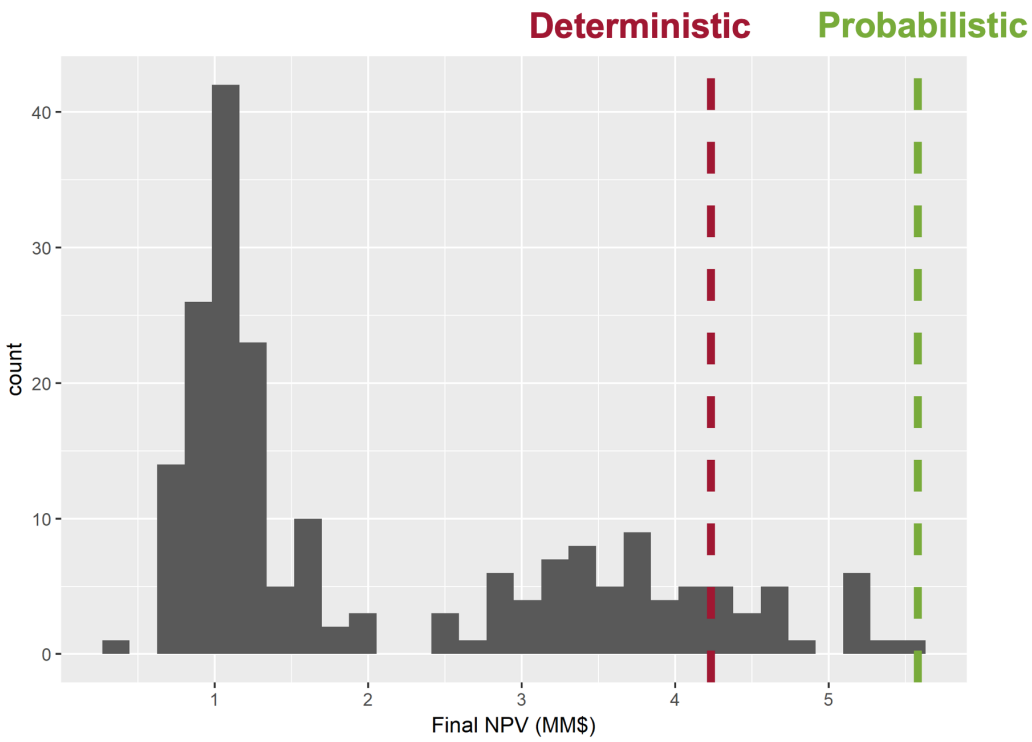

Figure 2.22: NPV Validation of Injection Schemes' Optimality

2.5 Conclusion & Future Works

Chapter 2 proposed a workflow designed to find the optimal injection scheme in a waterflooding scenario. The workflow has employed a combination of two simple models (CRMP and Koval) in conjunction with a method to generate a stochastically diverse history matched models (bootstrap), a robust optimizing algorithm to determine the injection rates (EnOpt), and a sampling method (Thompson sampling). The selected injection schemes were then validated using a commercial, discretized reservoir simulator that was assumed to be the true case.

The demonstration employed the CRMP & Koval models, which are very light in computational cost. However, this workflow's value increases as does the simulation time required for one realization. Instead of optimizing the injection rates using the discrete reservoir simulation models, which will require much repetitive and mostly unnecessary computations (unnecessary because the results will be discarded), we should use another layer of simple models to converge to a set of decisions that are most likely to yield the highest returns. Reservoir engineers can then apply the Thompson sampling scheme to determine the injection scheme that is the most likely to yield the highest returns.

Chapter 3

Real Options Valuation of a Refrac Candidate Well Using Least-Squares Monte Carlo

Real options are decisions a manager can make during a project's life in response to changing economic, technological or market conditions (Dixit and Pindyck, 2012). The decisions often have the potential to introduce significant changes to a project in terms of risks, cash flows, and sizes. The challenge presented to the decision-maker is to systematically take into account the current and future uncertainties, as well as the decisions available, to maximize the value of the project. Such challenges are inherent in managing many different types of assets and financial instruments, such as equity, commodity, foreign exchange, insurance, energy, sovereign, agency, municipal, mortgage, credit, real estate, convertible, swap, and emerging markets (Longstaff and Schwartz, 2001).

The wide range of applicability of real options has given rise to just as diverse real option valuation methods. Because it is often difficult to find a closed-form solution to a real options valuations problem, many of the proposed solutions involve numerical methods. Numerical methods facilitate incorporating multiple underlying variables and models. The methods are broadly

categorized into three groups: simulation methods, lattice methods, and finite difference methods. Simulation methods involve generating multiple Monte Carlo realizations to represent the uncertainties in different variables and their interactions. Lattice methods discretize the time until the option's expiration and map out the possible exercise scenarios. Finally, finite difference methods find a numerical solution to partial differential equations describing the price of derivatives.

The benefit of employing a real options approach to valuation is evident when the method is compared against the more traditional discounted cash flow (DCF) method. In the more widely-implemented DCF method, a certain irreversible decision is assumed to be made at a time period with certain economic assumptions, and the subsequent cash flow is generated. The cash flow is then discounted using the interest rate and summed back to the time of decision, resulting in an NPV value. This value is then used as the basis for justifying one action over another.

While the DCF method is more commonly selected, it is not without limitations. For instance, when evaluating scenarios where a decision will be made in the future, the DCF method fails to account for the new information relevant to the decision that one will have acquired by the time he/she makes the decision. The shortcoming in this method of analysis is further exacerbated if the underlying economic factors are highly volatile and capital-intensive, as is often the case with petroleum assets (e.g. oil and gas prices). This is because the preference for different decisions and the managements' operating

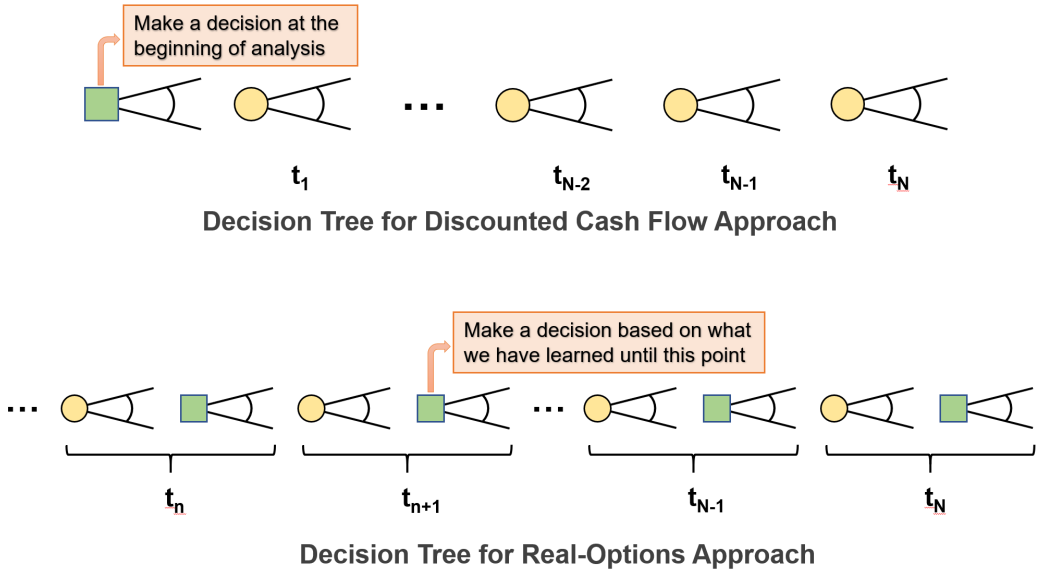

Figure 3.1: Discounted Cash Flow vs. Real Options Approach to Valuation

strategies are intricately related to how the market uncertainties resolve. The real options method provides a framework in which such responses to the resolution of uncertainties can be systematically integrated into the valuation process. Figure 3.1 is provided to help the reader visualize the difference between the two methods. Unlike the discounted cash flow approach, the decision tree for the real options method contains multiple decision nodes to represent multiple points in time where one can make a decision based on the information accumulated until that time.

This work incorporates the LSM method, which is one of many ways proposed to solve the real options valuation problem, to demonstrate the valuation process of a horizontal well which has the option of refracturing. Because the primary emphasis of this work is in illustrating how the real options ap-

proach to valuation provides a robust and versatile framework that allows the user to systematically incorporate multiple sources of uncertainty and the flexibility in decisions, the simulational aspects of refrac and recovery are simplified.

The many ways in which LSM is used is presented in the next section.

3.1 Literature Review

Least-Squares Monte Carlo (LSM) is a simulation-based solution to the real options valuation problem. It was first devised by Longstaff and Schwartz (2001) to help find an approximate solution to estimating the value of American options[1] using simulation. LSM evaluates the conditional expected payoff at each time step using least squares. Longstaff and Schwartz (2001) details the algorithm and provides multiple detailed examples in increasing degrees of complexity to demonstrate the application and versatility of the simulation method. The mechanics of the algorithm is established in section 3.2.1 of this dissertation also.

The use of LSM in petroleum engineering literature is only beginning to gain interest in recent years. This section of the literature review will examine the different ways in which LSM was employed to solve petroleum-related

[1] An American option refers to an option that can be exercised at any time before the expiration date. An alternative to the American option is the European option, which can be exercised only at the expiration date of the option.

problems.

Brandão et al. (2005) was one of the first works that proposed the use of real options valuation approach to estimate the value of an oil production project, with a scale option[2]. The work employs Monte Carlo simulations and binomial decision trees to model for the uncertainties in how the value of a project will evolve through time. Later in the same year, Smith (2005) put forth an alternative solution to Brandão et al.'s example problem by using the LSM. Smith's argument was that for scenarios where there are many underlying uncertainties, lattices or decision trees are susceptible to the curse of dimensionality; Longstaff and Schwartz's LSM method is the preferred solution because it allows easy integration of these uncertainties as long as the number of decisions remain small.

There are additional references in the petroleum literature that address different engineering problems using the LSM algorithm. For instance, Thomas and Bratvold (2015) determined the optimal time for gas blowdown for an oil field with gas caps or associated gas. The work compared the results from a "naive" Monte Carlo simulation valuation with the real options approach, and concluded that the latter has found the preferred decision. In their LSM implementation, the authors have included uncertainties in oil and gas reserves, production rates, and transition costs. They have paired it with a material balance simulator to predict oil and gas production. The paper

[2]Scale option refers to the ability to "increase or decrease one's interest in the investment in exchange for a cash payment of receipt." (Brandão et al., 2005)

recommends the use of real-options approach because it "better mimics actual information gathering and decision making" (Thomas and Bratvold, 2015), and it is indifferent to the number of uncertain factors in the analysis.

Hong et al. (2018) used a two-factor production model by (Parra-Sanchez, 2010), combined with LSM to determine the optimal time to initiate an improved oil recovery (IOR) process. The work introduces slight modifications to the original LSM algorithm proposed by Longstaff and Schwartz (2001) by relaxing the Markov assumption associated with the behavior of state variables (i.e. reservoir properties). The paper then compares the results with that from a closed-loop reservoir management framework, which does not take into account the potential impact of the future information relevant to the decision under consideration. The comparison establishes that the solution derived from the closed-loop reservoir management framework is indeed suboptimal, suggesting that a dynamic programming approach—such as LSM—can significantly improve the quality of decisions.

Willigers and Bratvold (2009) demonstrated an example of using LSM to determine a value of a gas field with two available options: to trade the produced gas on the spot market and to sell the gas through a supply contract. The work incorporates three factors, each associated with different uncertainty: the gas price, the operational costs, and the rate of production decline. The first two, the gas price and the operational costs, are assumed to be positively correlated to reflect historical trends. The paper discusses the advantages of real-option-valuation methods over the net present value approach, one of

which is that it incorporates the value of flexibility in a project.

3.2 Models, Methods, and Algorithms Used

This section will introduce the tools that were used to solve the problem of when to implement the hydraulic refracturing, given uncertain economic conditions. Least-Squares Monte Carlo (LSM) is used to establish the overall framework of analysis, the Ornstein-Uhlenbeck process is used to model for gas price, and ensemble Kalman filter (EnKF) is used to iteratively update the parameters of the price model given hypothetical price realizations.

3.2.1 Least-Squares Monte Carlo (LSM)

The Least-Squares Monte Carlo is a simulation-based approach intended to find an approximate solution to the real options valuation problem (Powell, 2011). Using its dynamic outlook, the algorithm integrates the flexibility of a project that will allow the decision-maker to adapt to the resolution of uncertainties to maximize the value. In the context of valuating an American option, for which the algorithm was originally devised, Longstaff and Schwartz (2001) describes it as follows: "[...] at any exercise time, the holder of an American option optimally compares the payoff from immediate exercise with the expected payoff from continuation, and then exercises if the immediate payoff is higher." In the LSM model, the expected payoff condi-

tional to the decision to continue is modeled using least squares. The least squares solution at every time step not only allows for an accurate estimate of option's value, but also serves to outline the optimal policy as a function of how the uncertainties resolve in the future.

As the name suggests, the LSM is largely in two parts: the Monte Carlo, and the least squares:

1. Monte Carlo simulation is used to stochastically generate multiple realizations of state variables.

    - State variables refer to factors in the analysis containing uncertainty.
    - If the state variables are expected to behave in a certain way (e.g. correlated or autocorrelated), then the realizations can be made to reflect these assumptions.

2. Starting from the last point in time and proceeding backwards, determine the optimal action at each time step.

    - The optimal action is determined using the option with the largest expected returns.
    - The expected returns is determined by regressing (using least-squares) the simulated returns to realizations of state variables.
    - The analysis begins from the end point and proceeds in reverse time order because at each time step, the availability of the exercise option is contingent on that the option was not previously exercised.

Additional detail regarding the mechanics will be provided using an example in section 3.3.3.

There are many reasons why the LSM algorithm is a suitable solution to this problem. First, LSM provides a general, versatile framework with which analysts could use to incorporate multiple uncertainty factors without suffering the curse of dimensionality (Smith, 2005). The use of LSM is made possible because the number of options considered at every time step is small (refrac or continue production). More generally, choosing the real options approach to valuation is beneficial because it is able to accurately reflect the value of managerial flexibility. The fact that the product of analysis includes the optimal choices as a function of the resolution of uncertainties, as well as an accurate valuation, compounds to the reasons for selecting this approach.

As advantageous as it is to choose the LSM for this analysis, alternatives exist. The suitability of the algorithm in solving a real options valuation problem depends generally on the following: 1) whether a stochastic differential equation exists that accurately describes the system, 2) the number of decisions considered, and 3) the number of uncertainties to be included in the valuation. Other details such as path-dependence[3] can also affect the choice of algorithm. If the system can be easily described using a stochastic differential equation, finding a more immediate solution to the equation may be preferred over taking a more simulation-based approach. If there are path-

[3]Path dependence refers to how the availability or optimality of decisions are contingent upon the decisions previously made or the events previously transpired.

dependent aspects of economics that should be included, then a lattice- or decision tree-based model may be preferred.

3.2.2 Ornstein-Uhlenbeck Process

The framework of analysis established by the LSM valuation method involves generating many hypothetical future economic scenarios. Because the gas price is closely interrelated with the economics of the decision, it is important to select the model that accurately captures the price behavior. In this study, the Ornstein-Uhlenbeck process is used to model for gas prices' change through time. The model's parameter is estimated by sequentially updating the model parameters using the ensemble Kalman filter (EnKF) over historical Henry Hub gas spot prices. The data set of historical Henry Hub prices were monthly, end-of-the-month prices in the period from January 1991 to June 2017.

The Ornstein-Uhlenbeck process is advantageous because it provides a simple yet realistic way to capture the behavior of price through time. It is described by the following equation:

$$dx_t = \theta(\mu - x_t)dt + \sigma W_t \tag{3.2.1}$$

where

x_t: State variable undergoing Ornstein-Uhlenbeck process at time t

μ: Equilibrium, long-term value

σ: Degree of volatility around μ caused by shocks

θ: Mean reversion rate

W_t: Wiener-Lévy process (Brownian motion) $W_t = N(0,1)\sqrt{dt}$

Ornstein-Uhlenbeck process is mean-reverting. Mean reversion refers to the tendency of a state variable to eventually return to (and fluctuate around) a long-term mean. Such mean-reverting price models have been found to be appropriate for pricing many commodities (Dixit and Pindyck (2012), Smith and McCardle (1998)). The intuition behind mean-reverting processes is found in the way in which prices of commodities equilibrate through a simple dynamic between supply and demand (Schwartz and Smith, 2000). When the price of a commodity rises above the equilibrium level, the supply increases as a response because additional suppliers will enter the market. Increased supply will then cause the prices to decrease. On the other hand, when the prices are lower than the equilibrium price, then some suppliers will be forced to exit the market, inducing the price to rise. Depending on the market, the rate at which these events occur will vary, but in general the prices will tend towards the equilibrium at a rate proportional to the price's deviation away from its equilibrium (Begg et al., 2004).

Given the understanding of mean reversion in the Ornstein-Uhlenbeck process, we can intuitively understand the model parameters. μ refers to the

long-term mean value to which the state variable will tend to return, σ refers to the extent of variability away from μ, θ refers to how fast the state variable will tend to approach μ, and W_t refers to the Brownian motion, accounting for the stochastic nature of the process.

Depending on the problem, other pricing models can be used in the place of the Ornstein-Uhlenbeck process. An example is Gibson and Schwartz's (1990) two-factor model, which models for the spot price of oil and the instantaneous convenience yield. Another candidate for the price model is by Schwartz and Smith (2000), who proposed a model that not only includes the Ornstein-Uhlenbeck process of short-term fluctuations and mean-reversion, but also longer-term changes to the mean to which the short-term fluctuations revert. The authors have used geometric brownian motion (GBM) to model for the long-term changes in commodity price.

3.2.3 Ensemble Kalman Filter (EnKF)

One of the main advantages of using the real options approach in valuation is that the user can account for what has been learned until the time of decision. Bayesian analysis is often used to update one's predictions and estimations as new observations are made on relevant state variables. In this study, the Kalman filter is used to update the parameters of the Ornstein-Uhlenbeck process model, i.e. reflect the learning that will have occurred after observing how the prices change through time. At the core of Kalman filter's

mechanism is sequential Bayesian updating, which is integral in the framework of real options valuation method.

The Kalman filter is a "recursive procedure for computing estimates of unobserved state variables based on observations that depend on these state variables" (Schwartz and Smith, 2000). At every iteration, Kalman filter estimates the current state using the most recent observations, predicts what the next observations will be given the current set of observations and estimated state, and compares the next set of observations to update the current estimation of state variables. The type of Kalman filter used for this study is called the ensemble Kalman filter (EnKF), which uses stochastically generated ensemble of states to approximate the covariance matrix in the standard Kalman filtering process.

The Kalman filter is selected for this process because it provides a systematic way in which the price model's parameters can be estimated in a reproducible way. According to West and Harrison (1997), the variance in the state variable estimates will asymptotically approach a value that is independent of particular sequence of observations or the assumed prior distributions of the model parameters. Another reason that makes the Kalman filter a suitable selection of model calibration tool is that it is iterative. As time progresses and new observations are made in sequence, Kalman filter provides a methodical and consistent way to introduce and incorporate new information to the body of pre-calibrated parameters. In other words, it is not necessary to re-calibrate the whole model using all the data simultaneously when new

data is acquired.

Kalman filter is not the only method available to estimate the price model parameters given historical data. The reader is directed to Begg and Smit (2007) for a comprehensive review of alternative methods to estimate pricing model parameters from historical prices, such as section, weighted section, moving window, and weighted moving window method. Dixit and Pindyck (2012) also discusses parameter extraction from futures and option data for modeling risk-adjusted value paths. Additional relevant references for the reader include West and Harrison (1997) and Harvey and Peters (1990).

3.3 Experiment Formulation

In this study, we apply the real options approach to valuate a refrac candidate horizontal well. The least-squares Monte Carlo (LSM) algorithm is used to find an approximate solution to the dynamic programming problem that the real options method poses. The results section (3.4) will then discuss the advantages of using LSM, which are twofold: 1) accurate valuation of an asset that incorporates the value of flexibility, and 2) mapping of optimal policy as a function of the way in which uncertainties (random variables) resolve.

This portion of the dissertation will detail the way in which the problem is formulated to cultivate many advantages of real options valuation. Section 3.3.1 will review the reservoir simulation model designed to predict the gas production rate's response to refracs at varying time periods. Section 3.3.2

will then discuss how Ornstein-Uhlenbeck model is calibrated to historical Henry Hub prices, and the economic parameters used for this study. Finally, section 3.3.3 will discuss in detail how least-squares Monte Carlo algorithm is applied to determine the optimal policy, as well as provide an accurate valuation of the project that incorporates its flexibility.

3.3.1 Reservoir Simulation for Rate Response to Refrac

A reservoir simulation model is used to predict the gas production's response to refracs at different time periods. The reservoir model used for this study is simple because 1) the primary objective of the study is discussing the application of the valuation method and the determination of the optimal policy, and 2) the complexity of the reservoir is irrelevant to the discussion of the objectives.

As visualized in Figure 3.2, the reservoir model is only a portion of the total reservoir volume stimulated by existing and impending fractures. The resulting production rates are multiplied by the number of stages (15). The properties of the reservoir model is provided in Table 3.1. The model is homogeneous and isotropic, and one new fracture for every existing frac stage is simulated. The results of the simulation is provided in Figure 3.3. As the simulation results show, the model assumes that the refrac procedure and the corresponding rate response is instantaneous.

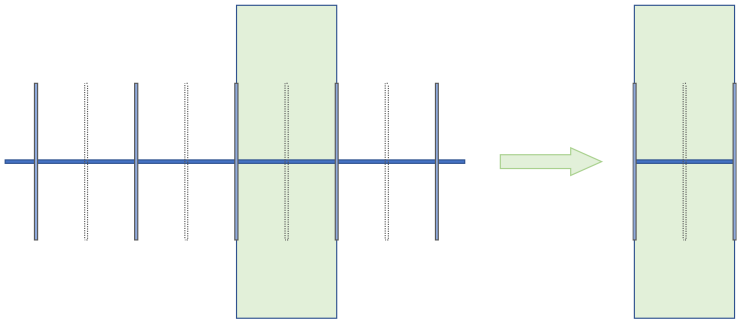

Figure 3.2: Sector Model of the Stimulated Reservoir Volume

Property	**Value**	**Unit**
N_x	120	-
N_y	100	-
N_z	1	-
dx	1	ft
dy	5	ft
dz	300	ft
L_x	120	ft
L_y	500	ft
L_z	300	ft
ϕ	0.06	
k	0.0003	mD
k_{frac}	50	mD
L_{frac}	300	ft

Table 3.1: Reservoir Simulation Model Properties

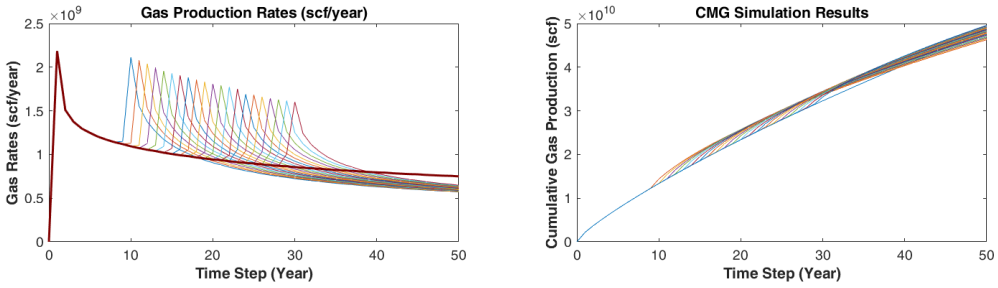

Figure 3.3: Gas Production Rates and Cumulative Gas Production Simulated with Refracs at Varying Years

3.3.2 Price Model Calibration & Economic Parameters

The next step is to use the ensemble Kalman filter (EnKF) to calibrate the Ornstein-Uhlenbeck model parameters. Historical Henry Hub prices from 1991 through 2017 are used to calibrate the parameters of Ornstein-Uhlenbeck model. Figure 3.4 displays the 80% confidence interval of stepwise EnKF prediction of the Henry Hub prices as it iteratively updates the model parameters. The three histograms in Figure 3.5 show the distribution of model parameters after the final time step of calibration. 100 ensemble members were used for EnKF. The mean values of each histogram in Figure 3.5 is selected as the final calibrated parameters for the price model.

Once the Ornstein-Uhlenbeck process is calibrated with the historical Henry Hub prices, 200 price path forecasts are generated, as shown in Figure 3.6. The values visualized in the figure will serve as the price projections from which the LSM algorithm will learn. The "learning" process is also done using EnKF, and is discussed in the LSM discussion section (section 3.3.3).

Table 3.2 lists the economic parameters used for the analysis. These

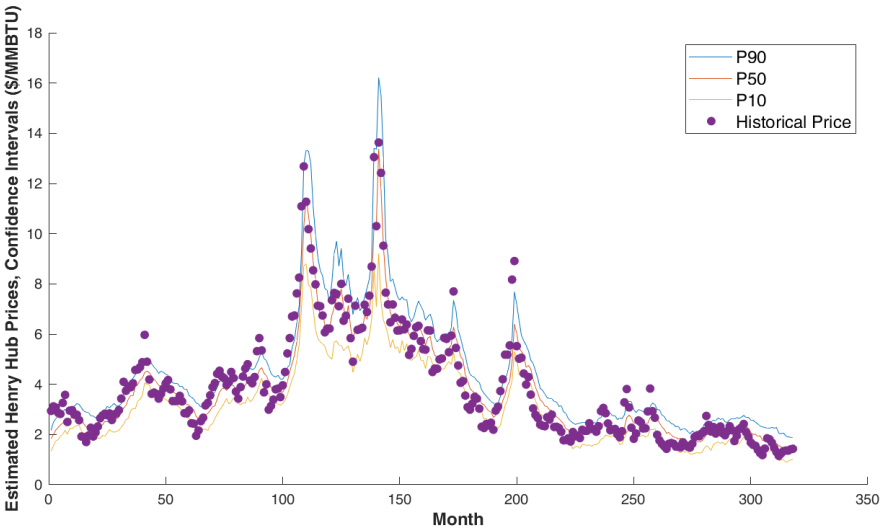

Figure 3.4: Ensemble Kalman Filter's Calibration of Ornstein-Uhlenbeck Model Parameters using Historical Henry Hub Prices from 1991 through 2017

values are assumed to be fixed.

3.3.3 Least-Squares Monte Carlo (LSM)

Now that the stochastic price model is calibrated and the economic conditions are established, Least-Squares Monte Carlo (LSM) is used to determine the optimal policy as a function of the resolution of stochastic variables

Economic Parameter	**Value**
Hydraulic Fracture CAPEX	8 MM$
Hydraulic Refracture CAPEX	7 MM$
Pre-Refrac OPEX	2 MM$
Post-Refrac OPEX	2.5 MM$
Annual Discount Rate	5%

Table 3.2: Economic Parameters Used for Refrac Timing Decision Analysis

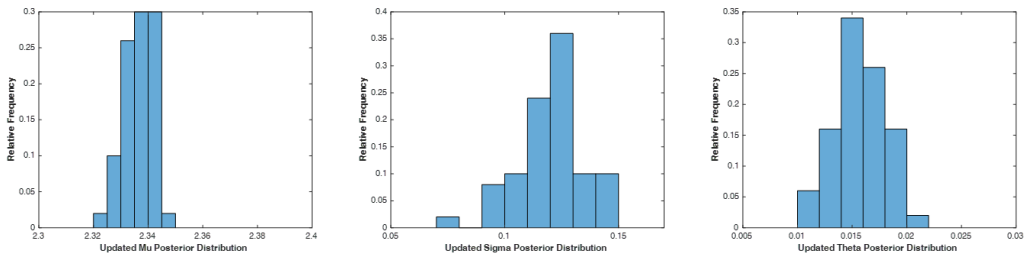

Figure 3.5: Calibrated Values of Ornstein-Uhlenbeck Model Parameters (μ,σ, and θ)

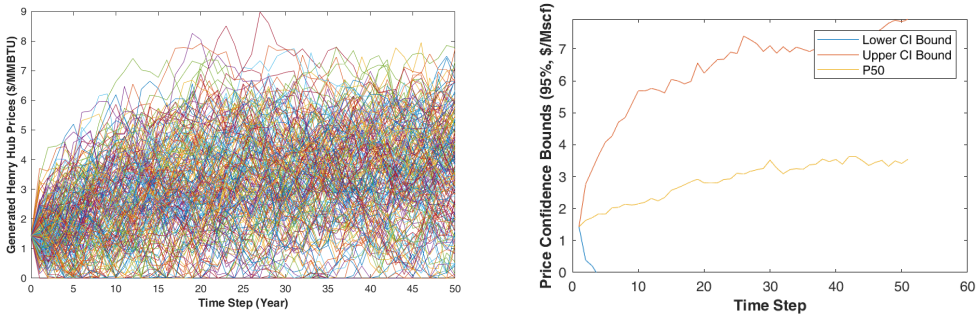

Figure 3.6: Gas Price Path Realizations with EnKF-Calibrated Ornstein-Uhlenbeck Model (Individual Realizations & 95% Confidence Interval, with P50)

in the analysis. At every time step between years 10 and 30, three options are considered: continue production without refrac, refrac the well and resume production, and terminate production. Beginning at year 30 and proceeding in reverse temporal order, the following sequence of computation is executed:

1. EnKF is used to update the Ornstein-Uhlenbeck model parameters using the price path generated, which is previously shown in Figure 3.6. This is an important step in the LSM algorithm that simulates the learning that will have occurred in the hypothetical scenario where the generated price path is true.

2. Using the Ornstein-Uhlenbeck price model calibrated in step 1, generate a price path realization 20 years into the future.

3. Using the price path generated in step 2, the simulated production response to refrac and the economic parameters, calculate the cash flow during the next 20 years, and convert it to NPV at the current time step using the discount rate. NPV is calculated using one of the following equations, depending on the option:

$$NPV_{t+1,continue} = \sum_{j=t+1}^{t+20} \frac{(q_{gas,continue,t}\$_{gas,t} - OPEX)\Delta t}{(1+r)^{j-t}} \tag{3.3.1}$$

$$NPV_{t+1,refrac} = \sum_{j=t+1}^{t+20} \frac{(q_{gas,refrac,t}\$_{gas,t} - OPEX)\Delta t}{(1+r)^{j-t}} - \$_{refrac} \tag{3.3.2}$$

$$NPV_{t+1,end} = 0 \tag{3.3.3}$$

$q_{gas,t}$: Gas production rate at time t, with or without refrac [scf/year]

$\$_{gas,t}$: Gas price [$/MMscf]

$\$_{refrac}$: Refrac cost [$]

$OPEX$: Annual operating expense [$/year]

Δt: Time interval [1 year]

r: Interest rate

t_{switch} : Optimal refrac time

4. For each option, regress the realized gas prices and production rates to NPV using a linear basis function to determine the optimal policy as a function of realization of uncertainties at the current time step. The linear basis functions for each option are provided below.

$$NPV_{t+1,continue} = a_0 + a_1 q_{gas,t} + a_2 \$_{gas,t} \tag{3.3.4}$$

$$NPV_{t+1,refrac} = b_0 + b_1 q_{gas,t} + b_2 \$_{gas,t} \tag{3.3.5}$$

$$NPV_{t+1,end} = 0 \tag{3.3.6}$$

5. Proceed to the previous time step (the algorithm proceeds in reverse temporal order) and repeat the above.

Iterating through the above five procedures through all the considered decision time steps (years 10 through 30) will result in the estimation of NPVs as a

function of the option (continue production, implement refrac, or terminate production) and the realization of uncertain variables, i.e. gas prices and production rates.

The results from completing the process listed in this section is provided in section 3.4.

3.4 Results

As discussed in the previous section, iterating through the LSM algorithm results in regressed models that provide estimates of the expected NPV (calculated using the 20-year cash flow following the decision) at every decision time step as a function of gas prices and production rates. As an example, the regressed linear models for year 10 are shown in Figure 3.7. The regressed models in the figure give expected returns associated with each decision at year 10. The figure can then be used to determine the optimal policy, depending on the future realization of the uncertain variables.

Figure 3.8 shows the regressed models for years 10, 20, and 30. The plot is shown from a bird's-eye view to delineate the optimal policy (the decision with the largest NPV) at every combination of gas price and production rates. The three cross-sectional view in time also demonstrate how the optimal policy changes through time.

There are apparent trends captured by the visualization of optimal

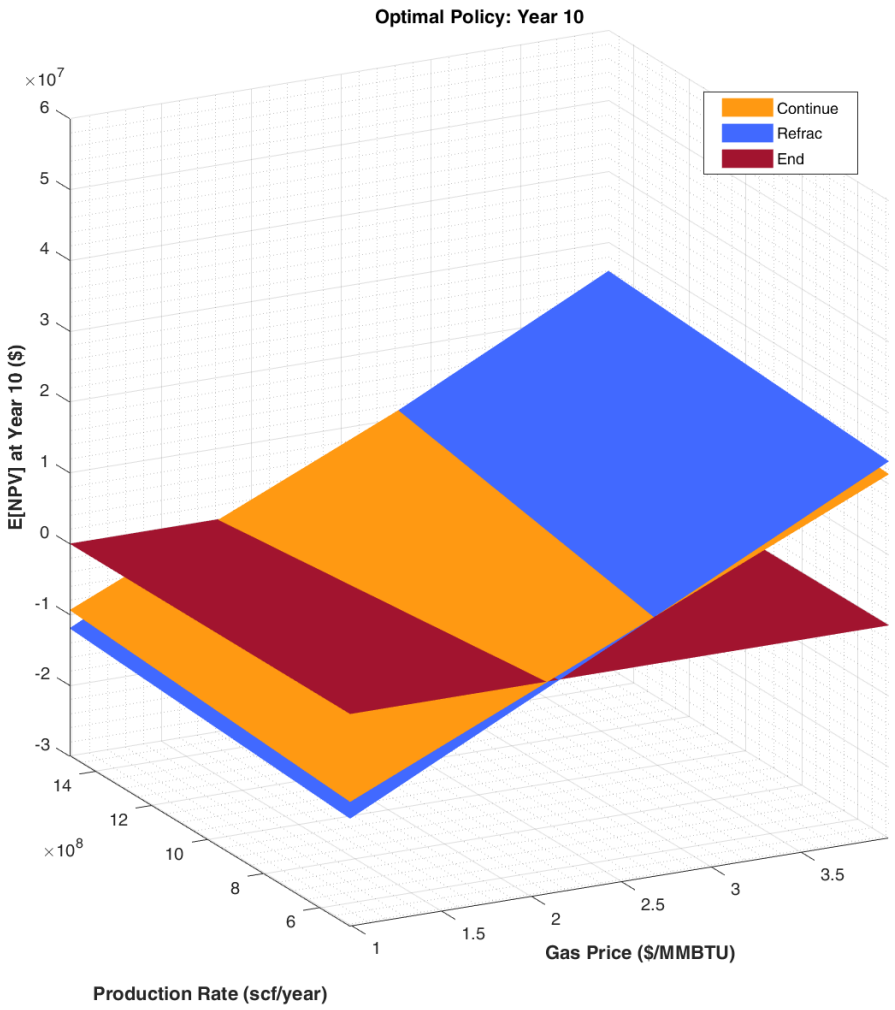

Figure 3.7: Least-Squares Approximation of NPVs of Three Options as a Function of Gas Production Rate and Gas Price at Year 10

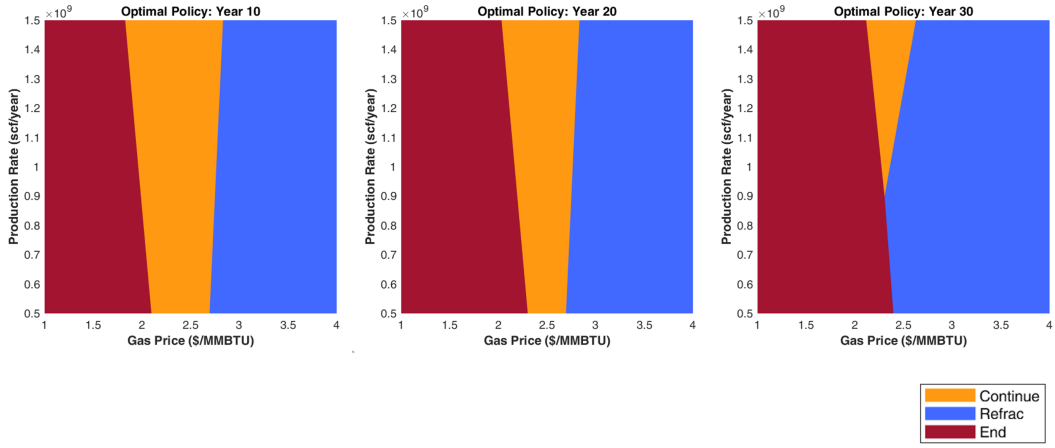

Figure 3.8: Visualization of Optimal Policies' Dependence on Realization of Random Variables at Years 10, 20, and 30

trends in this form. For instance, in Figure 3.8, the orange band is narrowing as the well matures. This indicates that as the well continues to produce, economic and physical conditions (i.e. gas price and production rates) wherein maintaining production is economic becomes increasingly constraining. The manager is slowly pushed to make a decision between refracturing the well and terminating the production. For instance, Figure 3.9 shows a hypothetical scenario where 800 MMscf/year production rates are observed at years 10, 20, and 30. The regions crossing the horizontal line indicate that, while for years 10 and 20, there exist ranges of gas prices where continuing production will be the most economic, the same is not the case for year 30. As such, the optimal policy generated using LSM is informed by the different stages of production the well is expected to undergo.

The slopes of the boundary lines between optimal policies yield inter-

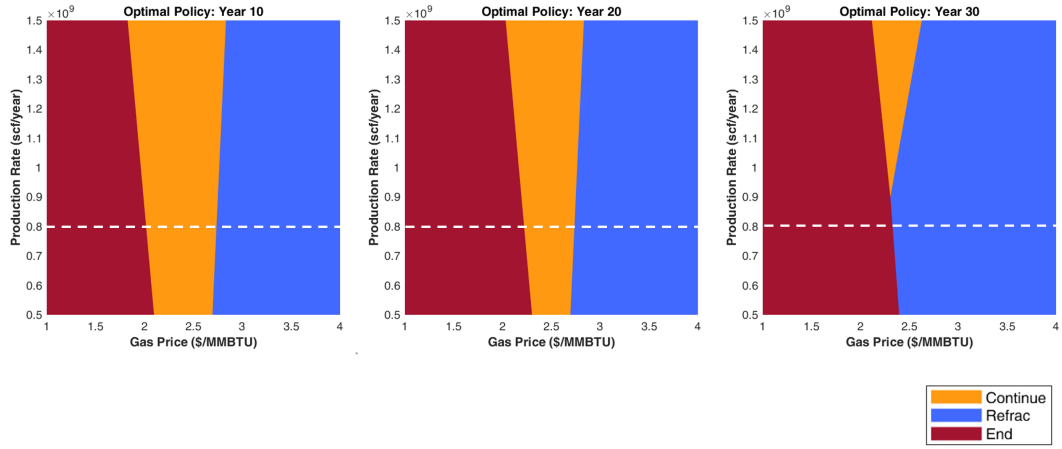

Figure 3.9: An Observation of the Optimal Policy at a Fixed Production Rate

esting insight into the problem. The boundaries are approximately vertical in Figure 3.8. Considering that the x and y ranges of the figure were selected to reflect the typical values we expect to see in the formulated problem, the steep boundary lines indicate that the future gas price has a much more significant role than the gas production rates in determining the optimal decision between continuing production, refracing, or terminating production. Generally, the larger the gas price, the more favorable it is to refrac the well or continue producing; this aligns with our intuition.

Despite their near verticality, the signs of the slopes of the boundary lines also coincide with what is expected. The terminate-continue (red-orange) line has a negative slope, indicating that the higher observed production rates tend to favor the decision to continue production. Similarly, the continue-refrac (orange-blue) boundary has a positive slope, showing preference for continuing production over refracing at high observed flow rates.

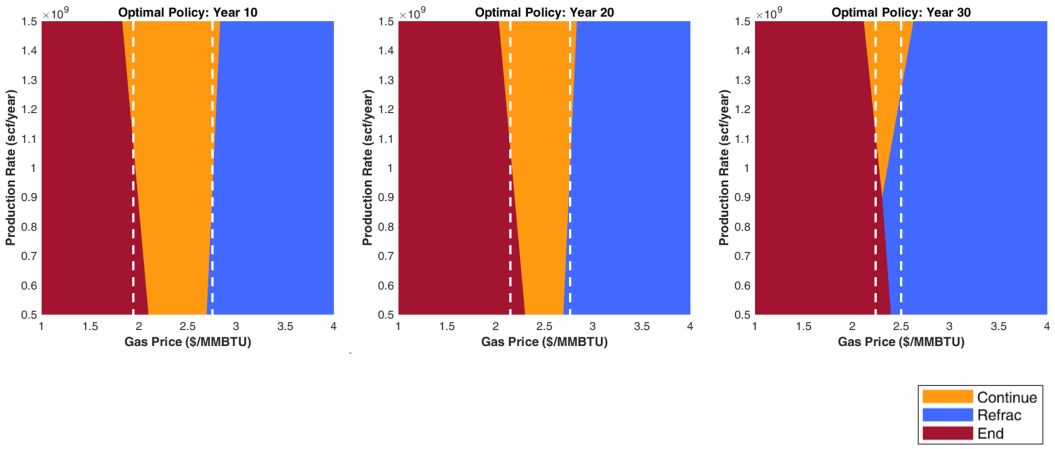

Figure 3.10: An Observation of the Optimal Policy at a Fixed Gas Price

A further observation in Figure 3.10 reveals that the slope of the threshold boundary lines between continue and refrac options (orange-blue) are almost nearly vertical in years 10 and 20, but has a more positive slope at year 30. This suggests that as the well matures and its productivity diminishes, the relative significance of the production rate in determining the optimal policy increases. The increased relative significance is related to the boundary line's deviation from the vertical line.

The optimal policies determined at every decision time step can now be used to estimate the value of the horizontal well. For each realized gas price path and production rates (for both continue and refrac), the valuation process will involve the following:

1. At each decision time step, take action as recommended by the regressed linear models and the simulated gas price and production rate.

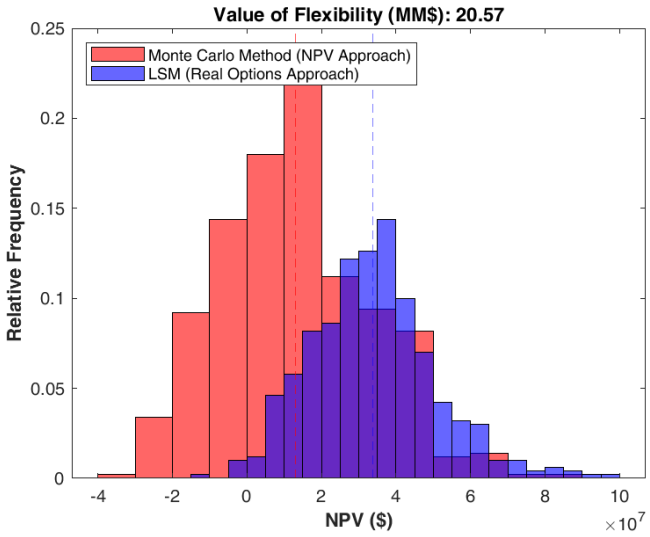

Figure 3.11: NPVs Estimated Using the Standard Discounted Cash Flow/Monte Carlo Method vs. Least-Squares Monte Carlo Method, and the Value of Flexibility

2. Determine the cash flow resulting from exercising the optimal policy at every time step.

3. Using the discount rate, determine the NPV.

4. Repeat above for all realized gas price paths and production rates.

Executing the procedure outlined above will result in a distribution of NPVs as visualized in blue in Figure 3.11. The expected value and the standard deviation of the NPVs determined in the figure are \$33.8MM and \$16.1MM, respectively.

This valuation result will now be compared against the NPV values estimated using a more myopic Monte Carlo and discounted cash flow (MC-

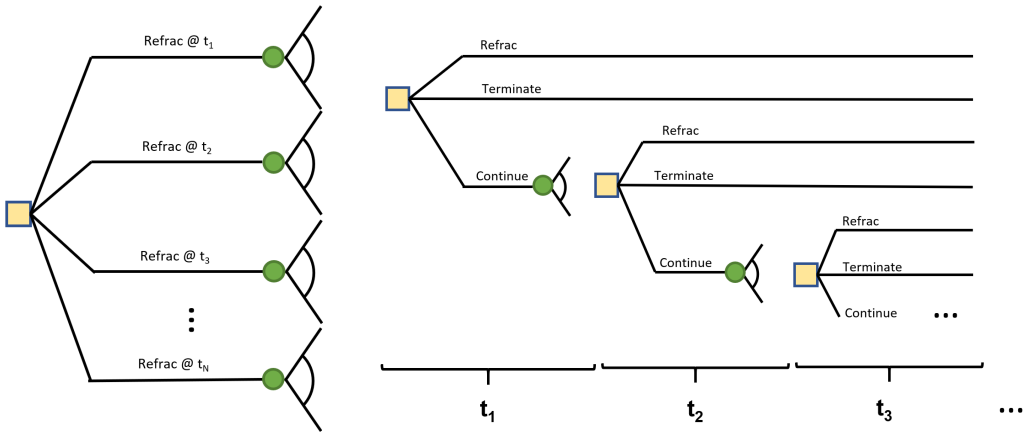

(a) Myopic MC-DCF Method

(b) Real Options Method

Figure 3.12: Decision Tree Schematics for MC+DCF and Real Options Method

DCF) method. The method uses Monte Carlo realizations of gas price paths and determines the present-day NPV distributions associated with refracing at every decision time step. The difference in the two methods is visualized using decision trees in Figure 3.12. As the first tree shows, the decision of when the refrac should be implemented is based only on the current estimation of uncertainties. The second tree better represents how decisions are made in reality because it includes the time-varying and learning aspects of decision-making. The manager is able to defer their decisions until a later time, and the real options method is able to account for the future learning that will occur if a decision is deferred.

In the Monte Carlo and discounted cash flow (MC-DCF) method, the optimal decision time is determined to be the period of refracing that yields the largest NPV, and the refrac is assumed to be implemented at this time.

The myopic DCF valuation implemented for comparison is calculated as:

$$NPV_{MC} = \sum_{t=1}^{T} \frac{(q_{gas,t}\$_{gas,t} - OPEX)\Delta t}{(1+r)^t} + \frac{\$_{refrac}}{(1+r)^{t_{switch}}} \tag{3.4.1}$$

$$t_{switch} = \underset{t}{\text{argmax}}[NPV_{MC}] \tag{3.4.2}$$

$q_{gas,t}$: Gas production rate at time t, with or without refrac [scf/year]

$\$_{gas,t}$: Gas price [$/MMscf]

$\$_{refrac}$: Refrac cost [$]

$OPEX$: Annual operating expense [$/year]

Δt: Time interval [1 year]

r: Interest rate

t_{switch} : Optimal refrac time

The distribution of NPVs resulting from the above calculations is visualized in red in Figure 3.11. The expected value and the standard deviation of the NPVs estimated using the Monte Carlo & DCF method are $13.2MM and $19.3MM, respectively.

The difference of the two expected values derived from real options and DCF valuations reflects the value of flexibility. Value of flexibility derives from splitting decisions into multiple decisions over time to allow learning in between decisions, resulting in better, more informed decisions (Bratvold

and Begg, 2010). In this problem, the value of flexibility is determined to be \$20.6MM (\$33.8MM−\$13.2MM). This corresponds to the value that the DCF method failed to take account of by ignoring the versatility of decision makers to respond to changing gas prices and production rates. As such, the LSM algorithm (and the real options approach) provides an accurate valuation method that is reflective of learning about uncertainties over time. Also, we have demonstrated that the LSM method also provides a valuable map of optimal policies through time.

Another way of understanding the value of flexibility is in Figure 3.11. It is apparent that the LSM valuation has a very small fraction of NPV realizations that are below zero. This is because the real options method allows for the possibility for the decision maker to take appropriate actions if the economic conditions are not favorable. Decision makers strive to minimize the downside and maximize the upside; the real options valuation method is able to reflect this in its valuations.

3.5 Conclusion & Future Works

This chapter demonstrated an application of real options method to determine the value of a refrac candidate horizontal well. Using the LSM algorithm, we were able to incorporate the flexibility of the project (i.e. continue production, implement refrac, or terminate production) as well as the future uncertainties associated with the gas price. The algorithm allows future

decisions to be based on what the manager will have learned by the decision time. The final product of implementing this method is 1) a map of optimal strategy through time contingent upon the future resolution of variables, and 2) an accurate valuation of the asset that reflects the flexibility available to the managers regarding the project.

There are many ways in which this work could be extended. Because the emphasis of this work was primarily in demonstrating how real options valuation approach provides a versatile framework that allows users to systematically integrate multiple information, the physical aspects of simulating the refrac and the corresponding gas recovery were greatly simplified. Incorporating either a more realistic representation of the complexities of a subsurface reservoir system, or a simple model that elegantly captures these complexities will further extend the validity and the utility of this approach.

Chapter 4

Infill Drilling Planning Using Monte Carlo Tree Search

In this chapter, we pair a reservoir simulation model with Monte Carlo tree search (MCTS) algorithm to optimize the infill drilling schedule. In a 2-dimensional reservoir simulation model, we will first delegate/identify candidate infill well locations in a grid-like structure. Then, using MCTS and multiple instances of reservoir simulations, we will 1) determine whether an infill well should be drilled at the specified candidate locations, 2) determine whether an injector or producer should be drilled, and 3) optimize the order in which the wells should be drilled. Economic parameters will be assigned to calculate the NPV, which is used as a measure of optimality of production schedules.

Additional detail regarding the problem formulation is provided in section 4.3. The next section discusses the relevant literature review.

4.1 Literature Review

Infill drilling refers to the addition of wells in a producing reservoir. Infill drilling reduces average well spacing while increasing sweep efficiency and estimated ultimate recovery. The decision regarding infill drilling involves determining whether additional drilling is economically justified, and, if so, when and where infill wells should be placed. This section will review some previous attempts either to identify locations for infill drilling or to optimize drilling and production schedules.

Chitsiripanich (2015) identified potential infill locations using CRM along with other reservoir characteristic properties such as porosity, thickness, and permeability. The author did so by visually comparing the CRM well connectivities and the spatial distribution of the bypassed oil in a mature water flooded reservoir, and also by qualitatively examining the well log data to identify locations of high permeability and large pore volumes. Chitsiripanich validated the method using simulated data, and also demonstrated its application to field data.

Weber (2009) studied injection well placement by using multiple traditional simulations to map out estimates of CRM parameters relative to pre-existing wells, and using the parameter map to conduct economic analysis to finally come to a recommendation of infill drilling location. Another method proposed by Weber uses logistic regression model to extrapolate the injector-producer well connectivity parameter to locations without wells.

Tavallali et al. (2013) generated a model that employs mixed integer nonlinear programming and honors the partial differential equations that describe reservoir dynamics. The model outputs the optimal number of infill producers, the locations of the producers, and optimal production plan.

Beckner and Song (1995) optimized the field development plan using simulated annealing on a reservoir simulator. The aspects of development included well scheduling and placement.

In this study, Monte Carlo tree search algorithm is used to optimize the infill drilling and production schedules. The mechanics of the algorithm is presented in the next section.

4.2 Models, Methods, and Algorithms Used

4.2.1 Monte-Carlo Tree Search (MCTS)

Monte Carlo Tree Search (MCTS) is a probabilistic tree search algorithm that uses repeated random sampling to estimate the value of actions as a game progresses. At every iterative state, stochastic sampling is used to update the estimates of the values of actions available at a given state, and the estimates are then used to expand the tree. Then, based on the expanded game tree, the next action is decided. As the algorithm continues to implement actions that are expected to be optimal, the process of traversing and expanding the tree is repeated at every iteration. MCTS is a probabilistic method because at the core of the algorithm, there is the stochastic sampling

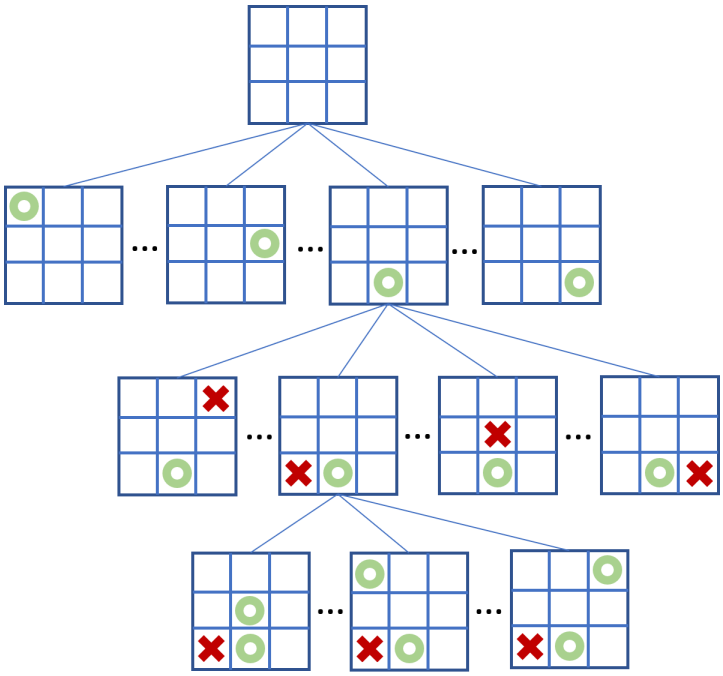

Figure 4.1: Monte-Carlo Tree Search Applied to Tic-Tac-Toe

that attempts to capture the response of actions without exhaustively examining them. Although it does not guarantee that it will find the optimal series of actions, many applications of MCTS in different fields have demonstrated that it is able to provide a close approximation of the optimal policy.

As the name suggests, MCTS involves a tree-like structure; it is used to represent different states and available actions. An example of a tree structure of a tic-tac-toe game is in Figure 4.1. In the diagram, the nodes represent different states that the tic-tac-toe board could take (nodes are more generally represented as a simple circle than a board). At the top of the tree, we start with the root node, with which represent the state of the board the game

begins. Given this state, the first player has nine different actions he can take. Four of the nine available actions are visualized in the figure. In the diagram, the available actions are represented using edges, which are the lines that connect the states. The states of the board resulting from these actions are represented using the child nodes. Four of the nine child nodes are shown in the figure in the second row as an example. Once MCTS carries out an action, then the corresponding child node becomes the new root node, and its sibling nodes would be discarded.

Each state carries with it an estimate of value that is calculated using Monte Carlo simulations. These values are then used to compare the quality of one action over another. Overall, MCTS consists of four stages: selection, expansion, simulation, and backpropagation. The four processes are repeated at every iteration, one of which is shown as an example in Figure 4.2. The two numbers in the nodes of the example tree represent the number of simulated wins and the number of simulations ("visits") that particular state has observed. The following sections will provide an overview of the mechanics of each stage using the example tree provided.

Selection

Selection process points the algorithm to which action is likely to be worth exploring. It takes the current state of the tree and selects decisions down that tree to a future state at a fixed depth. The relative value of different nodes are determined using the UCB equation (section 4.2.2), which system-

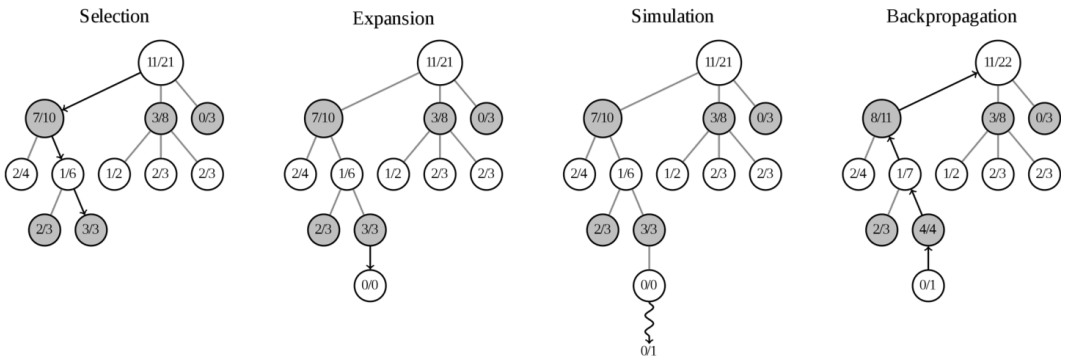

Figure 4.2: Four Stages in Monte-Carlo Tree Search Algorithm

atically incorporates both the observed average returns and the uncertainty associated with the estimated average.

Expansion

In this step, a new node is added to the tree as a child node of the node selected in the previous step. Only a single node is newly introduced to the tree at every iteration. In the figure, the expanded node has the numbers 0/0 because it has neither observed any wins nor simulations.

Simulation

The simulation step consists of randomly choosing moves until the algorithm reaches the terminal state or a specified threshold. Once the terminal conditions are met, then the algorithm calculates and returns a result of how well it performed as a score (in this work, the value is calculated from the

NPV). This score is then passed to the backpropagation phase. This stage relies on a forward model that provides us with the outcomes of an action in any state.

In this work, the optimality score is calculated using the NPV of the resulting cashflow. For the forward model, an open-source reservoir simulator called MRST is used.

Backpropagation

Once the value of the newly introduced node is determined in the simulation phase, the tree structure is updated. In the backpropagation step, the algorithm updates the perceived value of a given state, not just to the state it executed in the simulation but also every state that led to that state in the tree. The collection of the updated nodes can be observed by tracing the arrow that leads back up to the original parent node in Figure 4.2. This updating scheme allows the algorithm to search for early actions that may lead to opportunities that that may be observed in the future. The scores are updated until the root node (starting point) is reached.

Through the above four stages, we can take decisions to a fixed point in the tree, simulate their outcome, propagate back the perceived value of it. This process is repeated multiple times to balance out the optimal set of actions. Once the simulation count limit is reached, the algorithm chooses the optimal action leading to the state with the highest value.

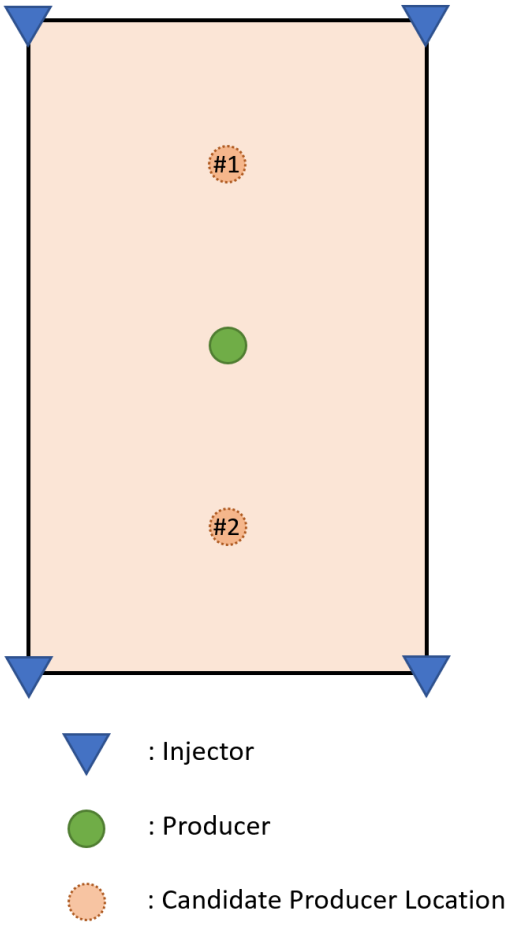

Figure 4.3: Simple Example Consisting of Four Existing Injectors and Two Infill Well Locations Analyzed Over Two Time Intervals (Candidate Locations Labeled)

To help the reader understand the problem formulation, a simplified version of the problem is provided. In Figure 4.3, we have a small reservoir system with four injectors and one producer. If there are two candidate locations for infill wells, and we are optimizing a schedule for the duration of two time steps, we can draw the decision tree as shown in Figure 4.4. Even with only a few candidate infill well locations and time steps, it is apparent from the figure that the decision tree has a very high branching factor. In other words, the challenge suffers from the curse of dimensionality. Despite this, the MCTS algorithm is able to determine a drilling and production schedule that is close to optimality. Additional detail regarding a more complex problem formulation is provided in section 4.3.

The following section discusses the Upper Confidence Bound (UCB) algorithm, which is the approach used in this work to guide the selection process of MCTS.

4.2.2 Upper Confidence Bound (UCB)

The upper confidence bound (UCB) is used in the MCTS's selection stage to traverse the tree. UCB is used to balance the selection process between exploration and exploitation. As described during the discussion of the multi-armed bandit problem in section 2.2.5, exploration and exploitation refers to the challenge posed to an agent to choose between acquiring new knowledge about the system and returning to an option that is expected to have large

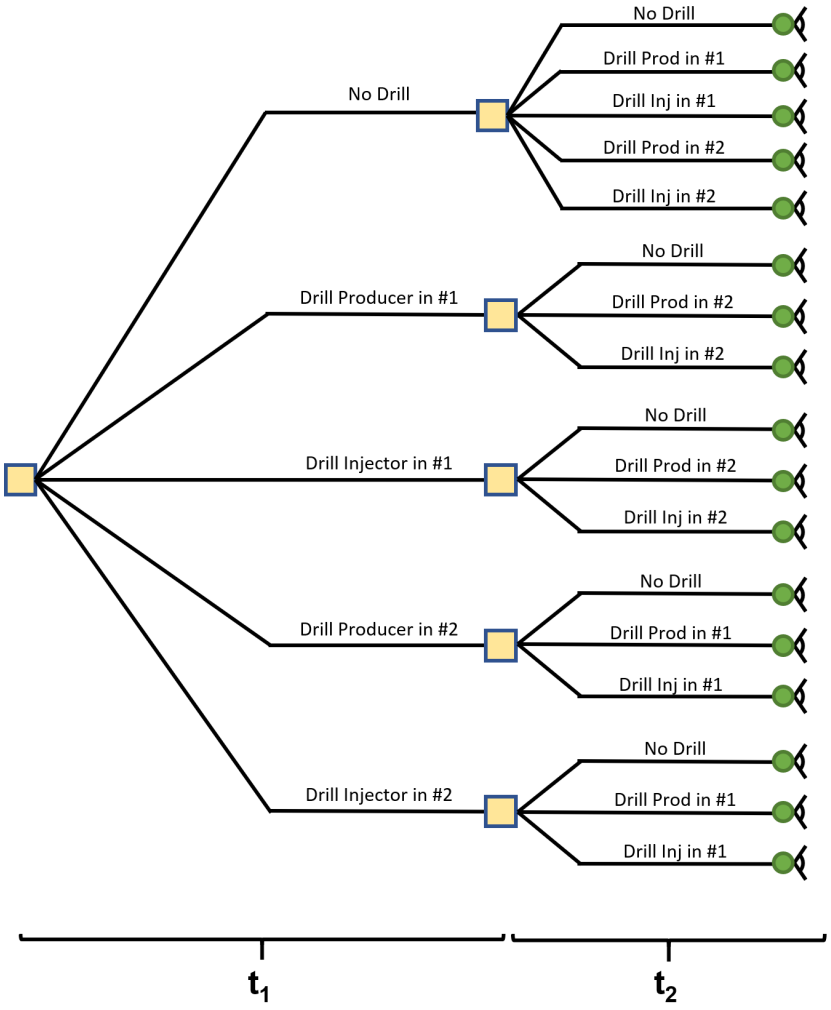

Figure 4.4: Decision Tree for Example Problem in Figure 4.3

returns, based on current knowledge. The UCB algorithm proposes that the agent pull the arm that maximizes the following:

$$UCB = \frac{\omega_i}{n_i} + c\sqrt{\frac{\ln N_i}{n_i}} \tag{4.2.1}$$

ω_i: Sum of returns or win count for the node after the i^{th} move

n_i: Number of simulations for the node after the i^{th} move

N_i: Total number of simulations after the i^{th} move

c: Exploration parameter; adjusts for exploration vs. exploitation

The above equation is intuitive. The $\frac{\omega_i}{n_i}$ term is the current estimate of returns associated with a decision. The remaining $c\sqrt{\frac{\ln N_i}{n_i}}$ term represent the upper bound of the confidence interval associated with the estimate, which is updated as the number of observations accumulate over time. The second term decreases as more observations are sampled to represent increased confidence in the expected returns.

The parameter c in the above equation controls for the extent to which uncertain options are favored. If c is set to zero, then the UCB algorithm would recommend that the agent pulls the arm solely based on the expected returns without considering the uncertainties associated with the estimations (i.e. exploitation). If c is set to a larger value, then the relative contribution of the expected value is reduced in the selection process, shifting the significance

more towards the uncertainties associated with estimates of expected returns. In other words, a UCB algorithm with a larger c tends to favor options that are not previously explored (i.e. exploration). An implementation of the selection process using the UCB equation will show that the algorithm will attempt to quickly identify the best alternative, and as it proceeds, it will keep searching for other good options while validating the optimality of the current "best".

4.3 Experiment Formulation

In this experiment, the MCTS algorithm (programmed in Python) will be paired with an open-source reservoir simulator (MRST) with pre-specified configuration of infill well locations to find the infill well drilling strategy that maximizes the net present value (NPV) of a field undergoing waterflooding. The reservoir model used is a 2-dimensional reservoir with $33 \times 33 \times 1$ grid count in x, y, z directions. The simulator is specified to use black oil, 2-phase, implicit solver to solve for fluid flow. Key properties of the reservoir model are listed in Table 4.1.

The porosity and permeability field is visualized in Figure 4.5. The correlation between the two variables and the histograms of each are provided in Figures 4.6 and 4.7, respectively. The reservoir model is made as sector model from the SPE-10 model (model 2) from the SPE Comparative Solution

Property	Value	Unit
N_x	33	
N_y	33	
N_z	1	
dx	25, 82	m, ft
dy	25, 82	m, ft
dz	50, 164	m, ft
L_x	825, 2706	m, ft
L_y	825, 2706	m, ft
L_z	50, 164	m, ft
μ_ϕ	0.26	
σ_ϕ	0.05	
μ_k	9.04	md
σ_k	1.51	md
$S_{w,init}$	0.3	

Table 4.1: Properties of the Reservoir Model Used for Infill Drilling Problem

Project[1].

The relative permeability model used for the simulation is the Corey-Brooks model, which uses a simple power-law relationship. It is shown below:

$$k_{ro} = k_{ro,max}(\frac{S_o - S_{or}}{1 - S_{or} - S_{wc}})^{n_o} \tag{4.3.1}$$

$$k_{rw} = k_{rw,max}(\frac{S_w - S_{wc}}{1 - S_{or} - S_{wc}})^{n_w} \tag{4.3.2}$$

The list of fluid and relative permeability model parameters are summarized

[1]The model can be downloaded from https://www.spe.org/web/csp/datasets/set02.htm

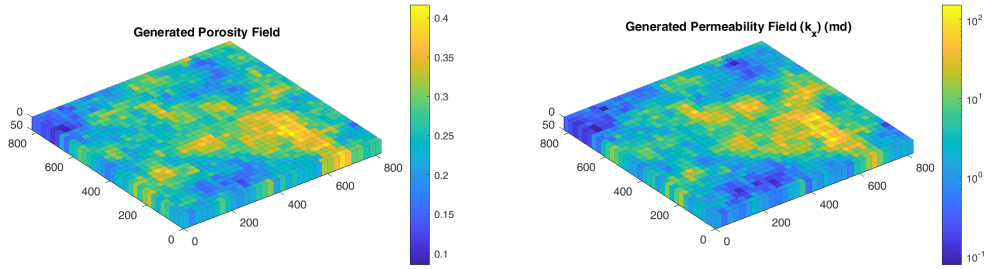

Figure 4.5: Generated Porosity and Permeability Fields

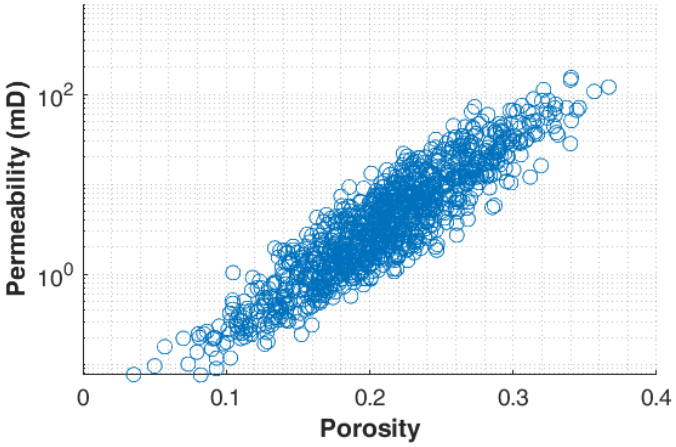

Figure 4.6: Porosity-Permeability Correlation

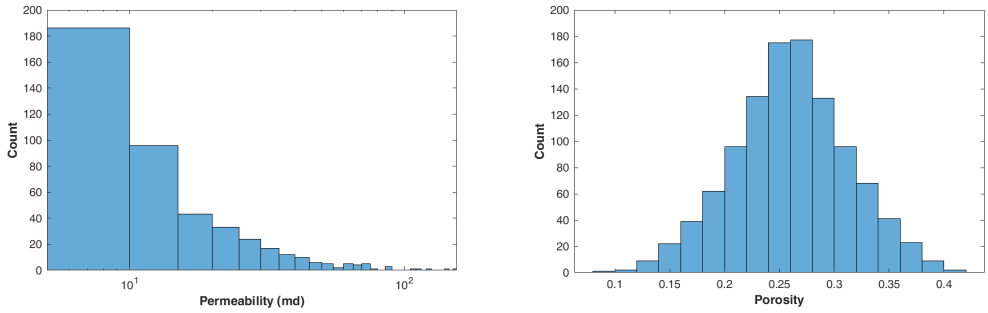

Figure 4.7: Histogram of Permeability and Porosity

Property	Value	Unit
μ_w	0.72	cp
μ_o	1.63	cp
ρ_w	1014	kg/m^3
ρ_o	859	kg/m^3

Corey-Brooks Model Parameter	Value
$k_{ro,max}$	0.8
$k_{rw,max}$	0.6
n_o	2
n_w	2
S_{or}	0.1
S_{wc}	0.2

Table 4.2: Summary of Fluid Parameters Used for Simulation

in Table 4.2. The relative permeability curves generated from the specified parameters are shown in Figure 4.8.

The following bullet points summarize the conditions with which the problem is formulated:

- There are five injector wells and four producer wells at current time (Year 0), as shown in Figure 4.9.
- 16 candidate infill well locations are specified using a grid-like arrangement, as shown in red in Figure 4.10.
- At every candidate infill well location, a producer or an injector can be drilled.

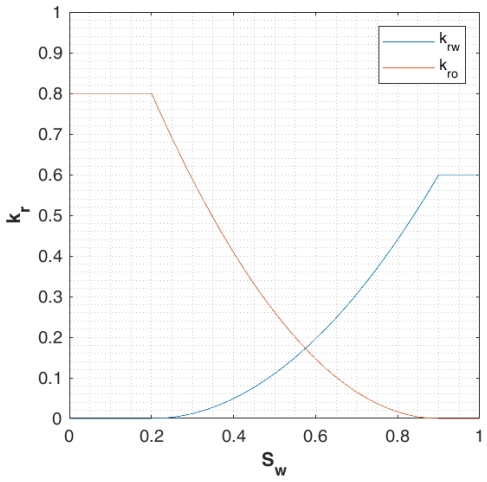

Figure 4.8: Relative Permeability Curve Generated Using Corey-Brooks Model

- The status of the well (injection or production) cannot be switched once drilled.
- Injection wells will maintain the injection rates at 250 STB/day, while the flowing bottomhole pressure of producers will be fixed at 1200 psia.
- Maximum of one well can be drilled in every year. The option to drill no wells is also available.
- Given the above conditions, the MCTS algorithm is to determine the optimal drilling schedule for the next 20 years that specifies the type, location, and the time to drill the infill wells.
- The optimality of a drilling schedule is calculated using the NPV, calculated using the following equation.

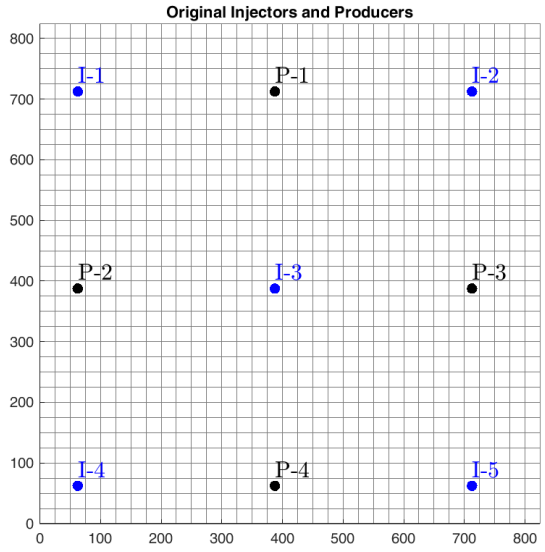

Figure 4.9: Existing Injectors and Producers (Axes in Meters)

$$NPV = \sum_{t=1}^{20} \frac{(q_{oil,t}\$_{oil} - OPEX)\Delta t - CAPEX_i}{(1+r)^t} \tag{4.3.3}$$

where $CAPEX_i$ is equal to \$10MM for years with new infill wells and zero for years without. Also,

$q_{oil,t}$: Oil production rate at time t, with or without refrac [STB/year]

$\$_{oil,t}$: Oil price [\$/STB]

$OPEX$: Annual operating expense [\$/year]

Δt: Time interval [1 year]

r: Interest rate

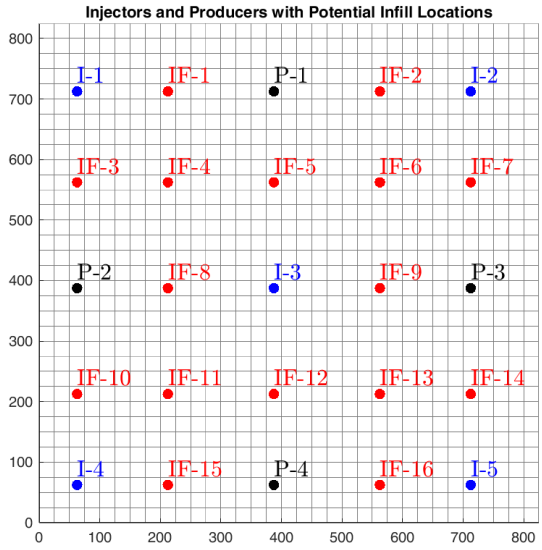

Figure 4.10: Candidate Infill Well Locations (Axes in Meters)

The economic parameters used for this study is summarized in Table 4.3.

Given the above setup, a conservative estimate of the total number of possible field development schedules can be calculated using a simple permutations formula

Economic Parameter	**Value**	**Unit**
Oil Price	50	$/STB
Injection Price	1	$/STB
OPEX	1	MM$/Year
CAPEX (Drilling)	10	MM$/Well
Annual Interest Rate	5	%

Table 4.3: Economic Parameters Required to Determine NPV

$$P(n, r) = \frac{n!}{(n-r)!} \tag{4.3.4}$$

where n is equal to the number of time steps considered, and r is the number of candidate infill well locations. The estimate of the number of different combinations, as calculated using the equation, is 1.01×10^{17}, which is prohibitively large. This number is an underestimate of the true count of possible combinations because it only includes scenarios where a well is always drilled at every time step; including the cases where drilling may be forgone will further increase this number. The MCTS algorithm will attempt to find the optimal strategy in a decision space that is intractably large.

4.4 Results

Using the setup detailed in the previous section, the MCTS algorithm was run to search for the optimal drilling and production schedule. MCTS parameters selected to are summarized in Table 4.4. The number of search paths and search depth is selected based on the simulation runtime; generally, the larger the number of these parameters, the longer the time it takes for MCTS to converge to an optimal solution. The overall runtime increases faster for increasing number of search paths than it does for search depth because increasing the search depth increases the number of time steps run in a simulation that is already running, while increasing the number of search paths increases the number of simulations altogether. The exploration constant (the

MCTS Parameter	Value
Number of Search Paths	100
Search Depth	5
Exploration Constant	10^7

Table 4.4: MCTS Parameters Used for Simulation

parameter c in equation (4.2.1)) is determined using the order of magnitude of returned NPV values, as well as trial and error.

The drilling schedule optimized by the MCTS paired with the reservoir simulator is visualized in a tabular form in Table 4.5. The table outlines the information about which wells should be prioritized for development. Locations indexed 2, 3, 4, 6, 8, 11, 12, 14, and 15 are recommended to have injectors drilled in different years, while the remaining locations are to be left without wells.

The optimized schedule consisting of drilling injection wells exclusively is interesting, given that the MCTS's search through decision space includes drilling both injection and production wells. The strategy overall suggests that the project is more likely to yield larger returns to push oil than to pull it. An abridged version of the full schedule is provided Table 4.6 for easier comparison with Figures 4.16, 4.17, 4.19, and 4.20.

Figures 4.11, 4.12, 4.13, and 4.14 represent the reservoir's response to implementing the MCTS-optimized production schedule. Note that in Figure 4.12, the negative production rates represent injections from the new injectors. For candidate locations that do not have a well, the rates remain at

	Active Infill Wells at Year:																				
Location Index	**0**	**1**	**2**	**3**	**4**	**5**	**6**	**7**	**8**	**9**	**10**	**11**	**12**	**13**	**14**	**15**	**16**	**17**	**18**	**19**	**20**
1	INACTIVE	INACTIVE	INACTIVE	INACTIVE	INACTIVE	INACTIVE	INACTIVE	INACTIVE	INACTIVE	INACTIVE	INACTIVE	INACTIVE	INACTIVE	INACTIVE	INACTIVE	INACTIVE	INACTIVE	INACTIVE	INACTIVE	INACTIVE	INACTIVE
2	INACTIVE	INACTIVE	INACTIVE	INACTIVE	INACTIVE	INACTIVE	INJ	INJ	INJ	INJ	INJ	INJ	INJ	INJ	INJ	INJ	INJ	INJ	INJ	INJ	INJ
3	INACTIVE	INACTIVE	INJ	INJ	INJ	INJ	INJ	INJ	INJ	INJ	INJ	INJ	INJ	INJ	INJ	INJ	INJ	INJ	INJ	INJ	INJ
4	INACTIVE	INACTIVE	INACTIVE	INACTIVE	INACTIVE	INACTIVE	INACTIVE	INACTIVE	INJ	INJ	INJ	INJ	INJ	INJ	INJ	INJ	INJ	INJ	INJ	INJ	INJ
5	INACTIVE	INACTIVE	INACTIVE	INACTIVE	INACTIVE	INACTIVE	INACTIVE	INACTIVE	INACTIVE	INACTIVE	INACTIVE	INACTIVE	INACTIVE	INACTIVE	INACTIVE	INACTIVE	INACTIVE	INACTIVE	INACTIVE	INACTIVE	INACTIVE
6	INJ	INJ	INJ	INJ	INJ	INJ	INJ	INJ	INJ	INJ	INJ	INJ	INJ	INJ	INJ	INJ	INJ	INJ	INJ	INJ	INJ
7	INACTIVE	INACTIVE	INACTIVE	INACTIVE	INACTIVE	INACTIVE	INACTIVE	INACTIVE	INACTIVE	INACTIVE	INACTIVE	INACTIVE	INACTIVE	INACTIVE	INACTIVE	INACTIVE	INACTIVE	INACTIVE	INACTIVE	INACTIVE	INACTIVE
8	INACTIVE	INACTIVE	INACTIVE	INACTIVE	INACTIVE	INJ	INJ	INJ	INJ	INJ	INJ	INJ	INJ	INJ	INJ	INJ	INJ	INJ	INJ	INJ	INJ
9	INACTIVE	INACTIVE	INACTIVE	INACTIVE	INACTIVE	INACTIVE	INACTIVE	INACTIVE	INACTIVE	INACTIVE	INACTIVE	INACTIVE	INACTIVE	INACTIVE	INACTIVE	INACTIVE	INACTIVE	INACTIVE	INACTIVE	INACTIVE	INACTIVE
10	INACTIVE	INACTIVE	INACTIVE	INACTIVE	INACTIVE	INACTIVE	INACTIVE	INACTIVE	INACTIVE	INACTIVE	INACTIVE	INACTIVE	INACTIVE	INACTIVE	INACTIVE	INACTIVE	INACTIVE	INACTIVE	INACTIVE	INACTIVE	INACTIVE
11	INACTIVE	INACTIVE	INACTIVE	INACTIVE	INACTIVE	INACTIVE	INACTIVE	INJ	INJ	INJ	INJ	INJ	INJ	INJ	INJ	INJ	INJ	INJ	INJ	INJ	INJ
12	INACTIVE	INJ	INJ	INJ	INJ	INJ	INJ	INJ	INJ	INJ	INJ	INJ	INJ	INJ	INJ	INJ	INJ	INJ	INJ	INJ	INJ
13	INACTIVE	INACTIVE	INACTIVE	INACTIVE	INACTIVE	INACTIVE	INACTIVE	INACTIVE	INACTIVE	INACTIVE	INACTIVE	INACTIVE	INACTIVE	INACTIVE	INACTIVE	INACTIVE	INACTIVE	INACTIVE	INACTIVE	INACTIVE	INACTIVE
14	INACTIVE	INACTIVE	INACTIVE	INJ	INJ	INJ	INJ	INJ	INJ	INJ	INJ	INJ	INJ	INJ	INJ	INJ	INJ	INJ	INJ	INJ	INJ
15	INACTIVE	INACTIVE	INACTIVE	INACTIVE	INJ	INJ	INJ	INJ	INJ	INJ	INJ	INJ	INJ	INJ	INJ	INJ	INJ	INJ	INJ	INJ	INJ
16	INACTIVE	INACTIVE	INACTIVE	INACTIVE	INACTIVE	INACTIVE	INACTIVE	INACTIVE	INACTIVE	INACTIVE	INACTIVE	INACTIVE	INACTIVE	INACTIVE	INACTIVE	INACTIVE	INACTIVE	INACTIVE	INACTIVE	INACTIVE	INACTIVE

Table 4.5: Optimized Infill Drilling Policy Table (Full)

	Active Infill Wells at Year:				
Location Index	**0**	**5**	**10**	**15**	**20**
1	INACTIVE	INACTIVE	INACTIVE	INACTIVE	INACTIVE
2	INACTIVE	INACTIVE	INJ	INJ	INJ
3	INACTIVE	INJ	INJ	INJ	INJ
4	INACTIVE	INACTIVE	INJ	INJ	INJ
5	INACTIVE	INACTIVE	INACTIVE	INACTIVE	INACTIVE
6	INACTIVE	INJ	INJ	INJ	INJ
7	INACTIVE	INACTIVE	INACTIVE	INACTIVE	INACTIVE
8	INACTIVE	INACTIVE	INJ	INJ	INJ
9	INACTIVE	INACTIVE	INACTIVE	INACTIVE	INACTIVE
10	INACTIVE	INACTIVE	INACTIVE	INACTIVE	INACTIVE
11	INACTIVE	INACTIVE	INJ	INJ	INJ
12	INACTIVE	INJ	INJ	INJ	INJ
13	INACTIVE	INACTIVE	INACTIVE	INACTIVE	INACTIVE
14	INACTIVE	INJ	INJ	INJ	INJ
15	INACTIVE	INJ	INJ	INJ	INJ
16	INACTIVE	INACTIVE	INACTIVE	INACTIVE	INACTIVE

Table 4.6: Optimized Infill Drilling Policy Table (Abridged Version of Table 4.5 for Comparison)

zero. In Figures 4.12, 4.12, and 4.13, we can see the step increase in production responses every time a new injector is introduced to the reservoir. Figure 4.15 visualizes the undiscounted cash flow at every time step of simulation; these values are used in conjunction with the discount factor to calculate the NPV. Because the simulation time steps are 0.1 year, the annual discount factor is converted accordingly.

The water saturation fields and the pressure fields for years 0, 5, 10, 15, and 20 are provided in Figures 4.16 and 4.17, respectively. The white space in the water saturation map represents the area that has not yet been sweeped by the injected water; the water saturation values in these regions remain at initial water saturation of 0.3.

In two-phase fluid flow in porous media, the mobility ratio can provide

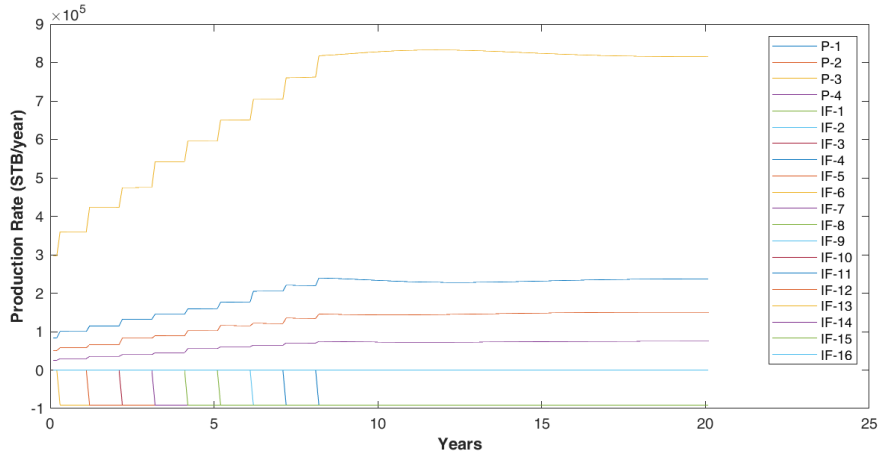

Figure 4.11: Fluid Production Rates for Existing Producers and Infill Wells (Negative Rates Indicate Injectors)

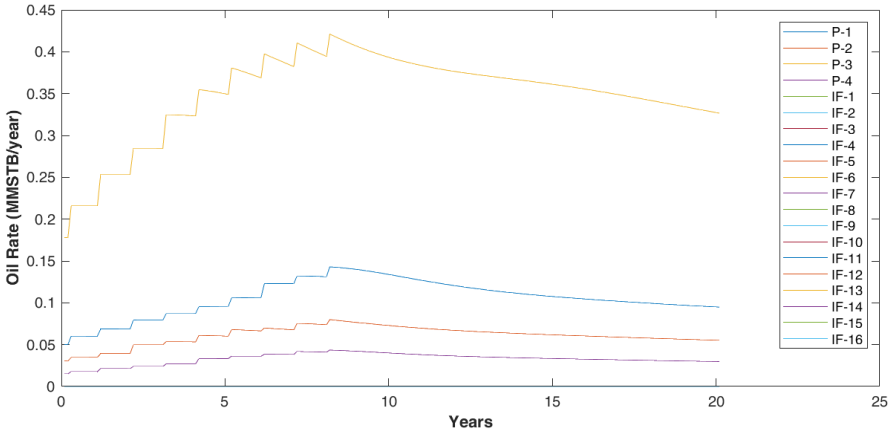

Figure 4.12: Oil Production Rates for Existing Producers and Infill Wells

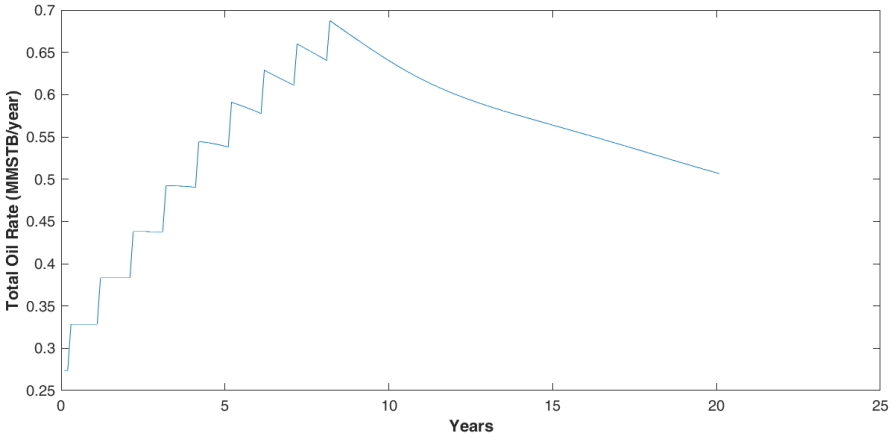

Figure 4.13: Field Total Oil Production Rates Through Time

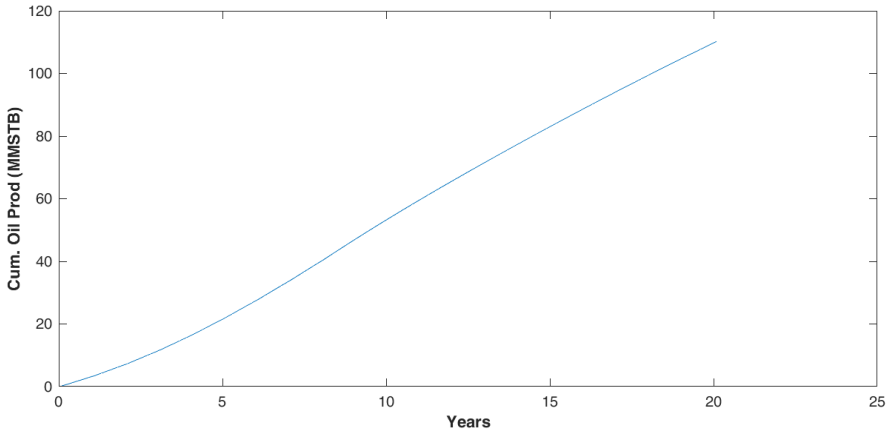

Figure 4.14: Field Total Cumulative Oil Recovery Through Time

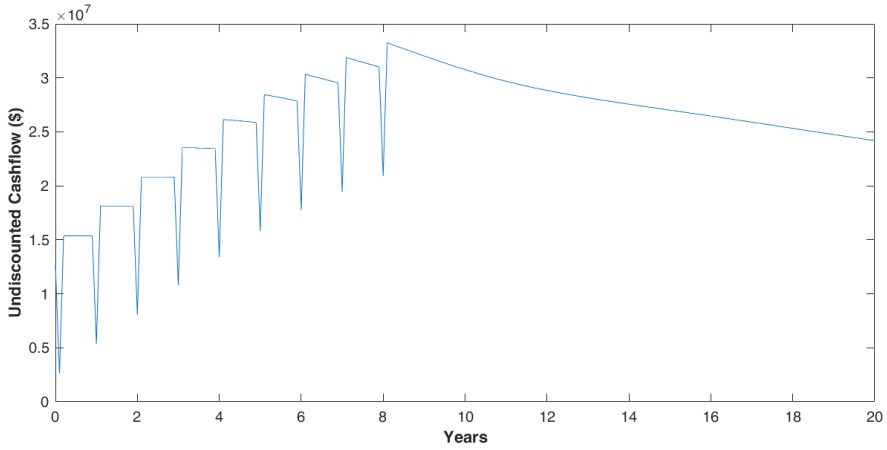

Figure 4.15: Undiscounted Cash Flow Through Time

a useful indicator for fluid displacement efficiency (Lake et al., 2014). The mobility ratio is defined as the mobility of the displacing fluid divided by the mobility of the displaced fluid. For waterflood, mobility ratio is

$$M = \frac{\lambda_w}{\lambda_o} \tag{4.4.1}$$

where $\lambda_w = \frac{k_w}{\mu_w}$ and $\lambda_o = \frac{k_o}{\mu_o}$. Substituting these equations and the relation of relative permeability to permeability ($k_w = kk_{rw}$ and $k_o = kk_{ro}$) in the above equation, we have the following.

$$M = \frac{k_w/\mu_w}{k_o/\mu_o} = \frac{k_{rw}/\mu_w}{k_{ro}/\mu_o} \tag{4.4.2}$$

Given that the relative permeabilities for oil and water is described by a power-law model (Figure 4.8), the mobility ratio can now be described as a function of water saturation. The relation calculated using the simulation parameters

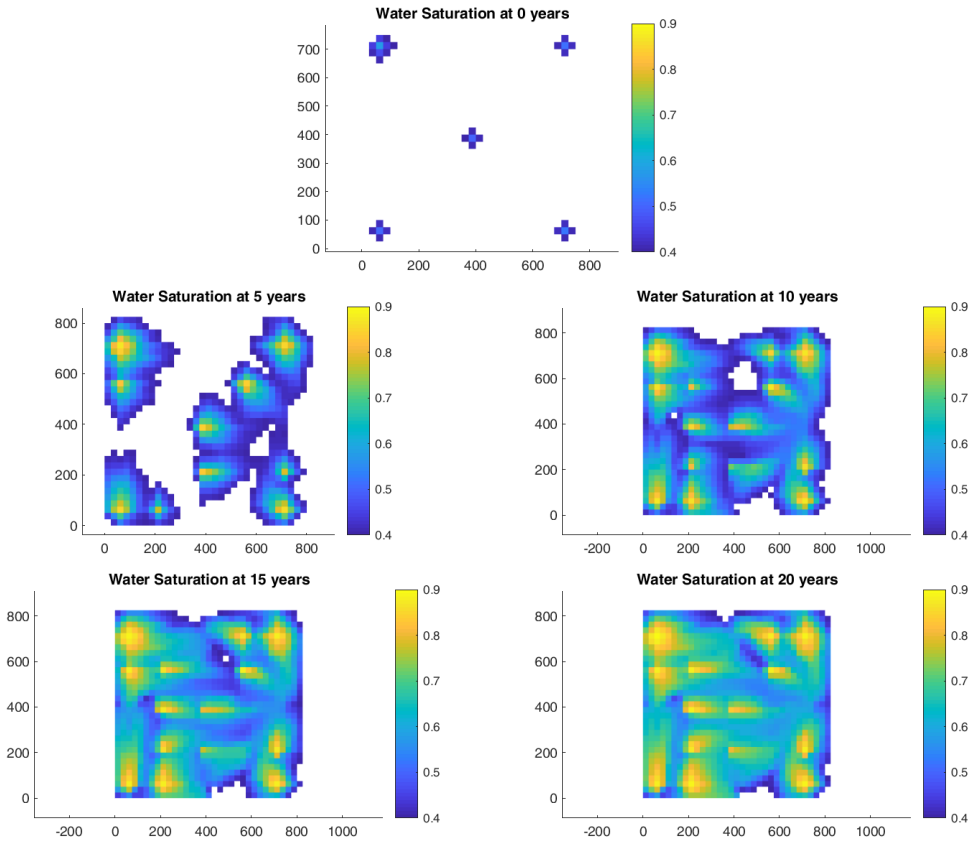

Figure 4.16: Water Saturation Field at Years 0, 5, 10, 15, and 20 (Axes in meters)

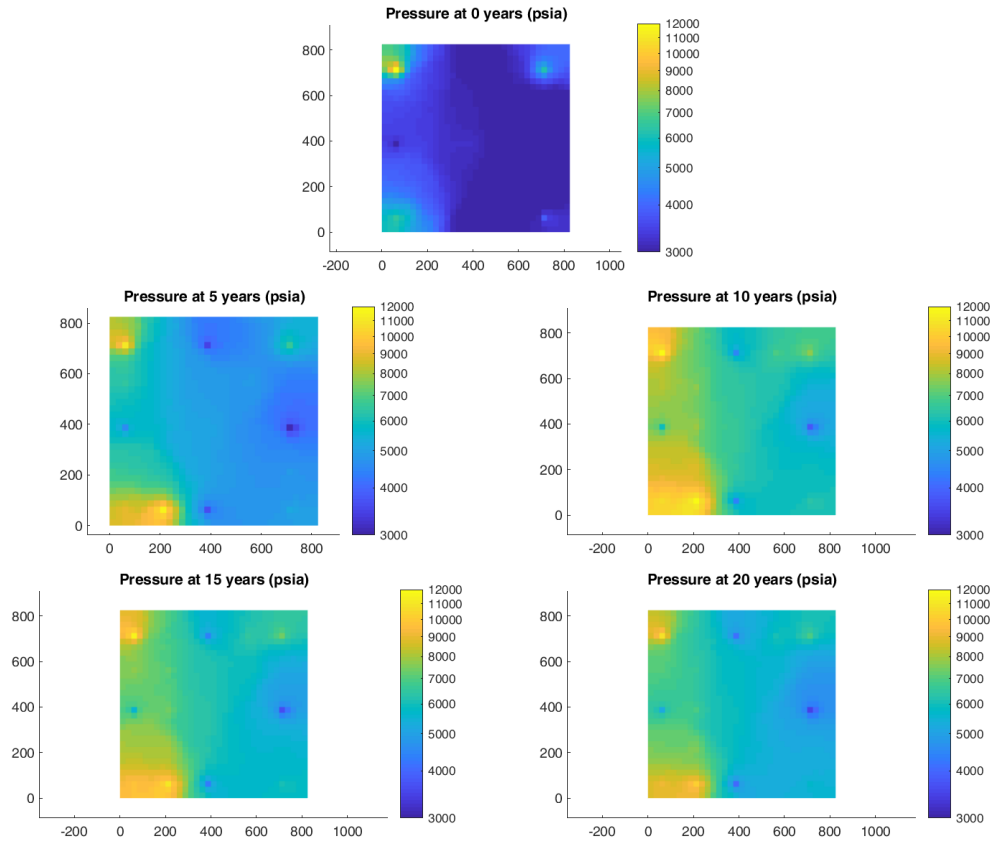

Figure 4.17: Pressure Field at Years 0, 5, 10, 15, and 20 (Axes in meters)

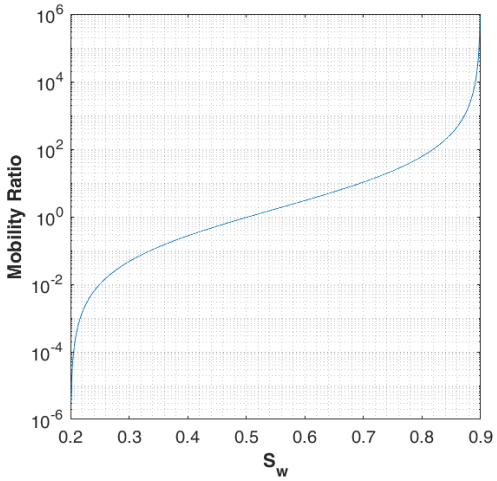

Figure 4.18: Mobility Ratio Calculated Using Relative Permeability Curves and Fluid Viscosities

is visualized in Figure 4.18. The evolution of mobility ratios through time in the simulation model is visualized in Figure 4.19. Also included is the map of regions where the mobility ratio is favorable for fluid displacement ($M < 1$).

4.5 Provisional Validation of Results

Because of the vast number of possibilities an infill drilling plan can take, it is impossible to prove that the final optimized plan determined by the MCTS algorithm is in fact a true optimum. Given this limitation, a partial validation will be provided by comparing the NPV and cumulative oil recovery resulting from the MCTS-optimized plan against those resulting from randomly generated infill drilling plans. 1000 random infill drilling plans were generated and was used in the simulator, resulting in a distribution of NPVs and cumu-

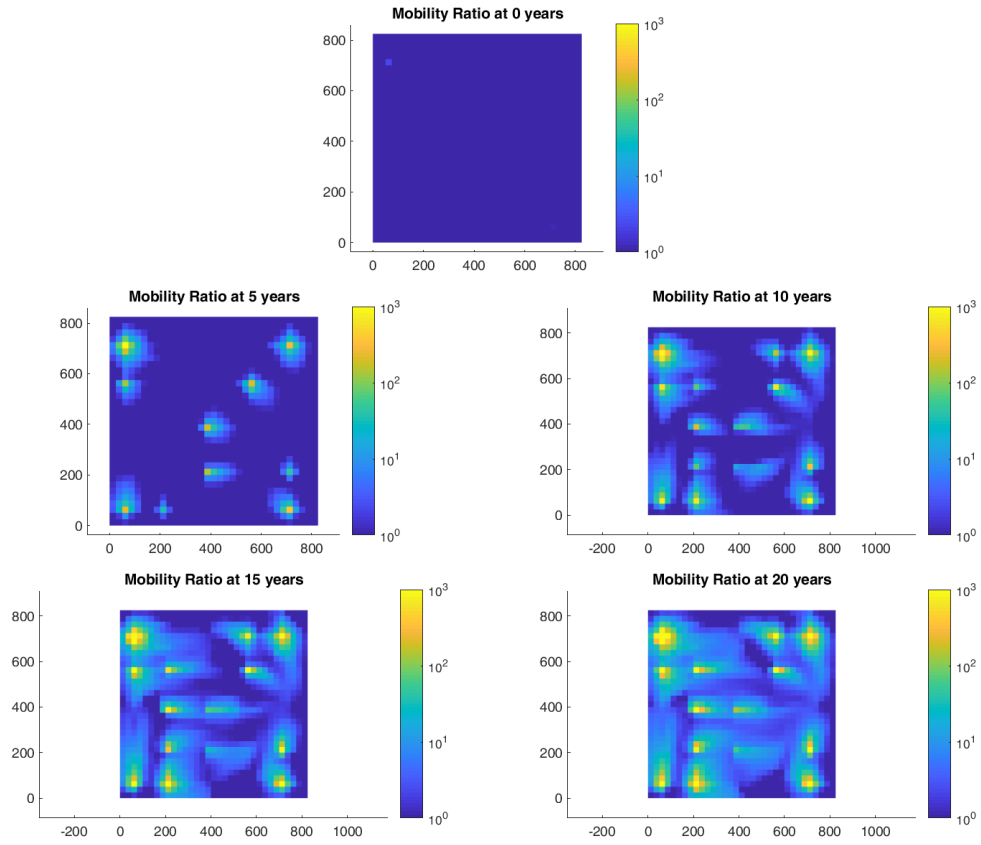

Figure 4.19: Mobility Ratio Field at Years 0, 5, 10, 15, and 20 (Axes in meters)

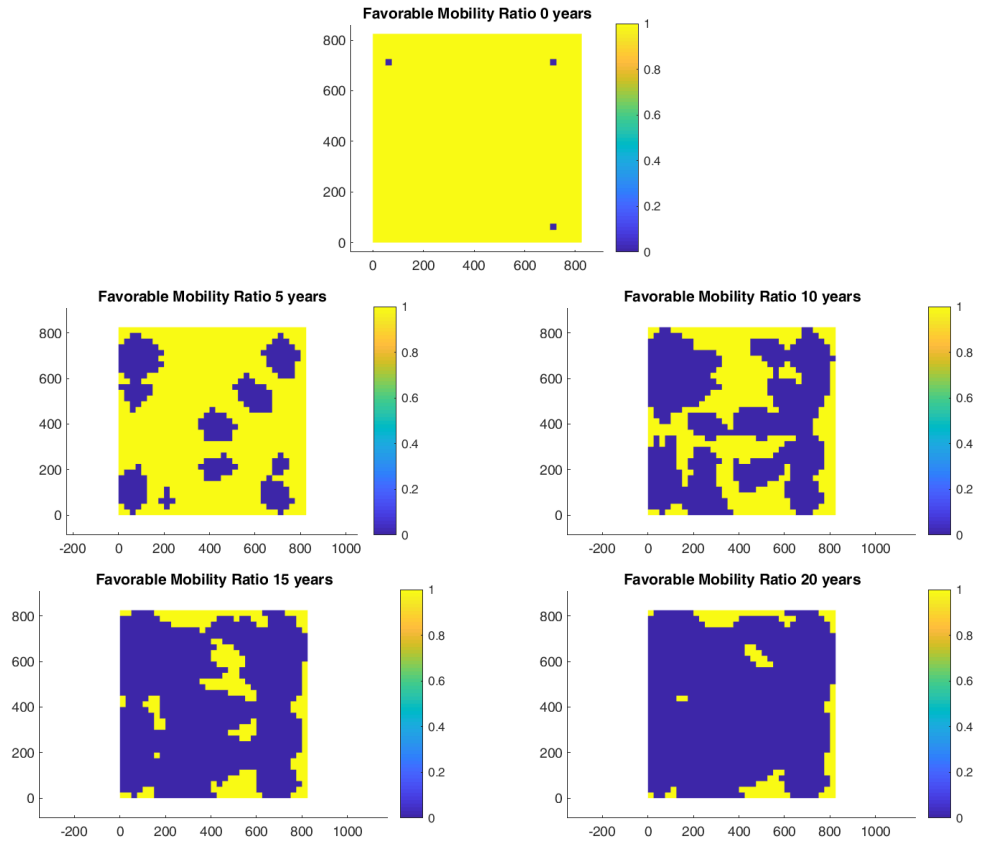

Figure 4.20: Favorable Mobility Ratio Field at Years 0, 5, 10, 15, and 20 (Axes in meters)

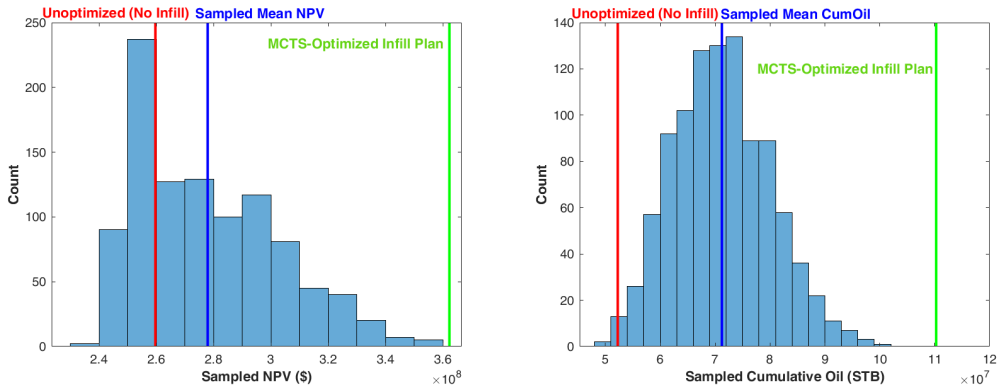

Figure 4.21: NPV and Cumulative Oil Recovered of MCTS-Optimized Plan and Randomly Generated Plans

lative oil recovery values. The generated distributions of NPV and cumulative oil recovery, and their mean values are visualized in the two histograms in Figure 4.21. The mean values of the distributions, the values corresponding to simulation with no infill wells, and the values from MCTS-optimized plan are also indicated for comparison. The specific numeric values are also summarized in Table 4.7. The NPV and cumulative recovered oil values indicate that the value of the MCTS-optimized plan far surpasses the expected NPV and oil recovery of randomly generated infill drilling and production schedules, which is expected. It is also interesting that none of the random schedules' NPV and recovered oil exceed those of the MCTS production portfolio, although a small number of random schedules come close. Although this is an imperfect method of validation, it nevertheless indicates that the MCTS-generated schedule is of value.

	No Infill	E[Random Schedule]	MCTS-Optimized Schedule
NPV (MM$)	259.68	277.91	362.24
Cum. Oil (MMbbl)	52.24	71.21	110.25

Table 4.7: Summary of Results

4.6 Conclusion & Future Works

This chapter proposed the Monte Carlo tree search (MCTS) algorithm as a solution to the problem of optimizing infill drilling schedule. The discussed method employs the MCTS in conjunction with a black oil reservoir simulator to stochastically search through the decision space to find a policy that is likely to yield the greatest return on investment. The versatility of the MCTS algorithm facilitates application to a diverse set of decisions that are sequence-dependent.

This application of MCTS to solve the infill well scheduling problem can be significantly improved by reducing the amount of computation required to approach an optimized policy. Because the MCTS algorithm calls upon the reservoir simulator multiple times to search for the optimal infill drilling schedule, the process can be computational- and memory-intensive, even with tree pruning.

A simple model that is able to predict the production responses at the candidate infill locations can be used in the place of the reservoir simulator. This replacement will allow higher resolution search in both time and space for the optimal schedule with available computational resources. Another advantage of developing a simple model is that it will allow the workflow to

stochastically represent the uncertainties associated with the reservoir model in forms of multiple realizations. To the author's knowledge, such simple model that does not rely on computationally costly reservoir simulators does not exist in the literature. section §5 outlines a beginning attempt to develop such a model based on the CRM model. Despite its incompleteness, it is nevertheless included in the dissertation as it may be useful for researchers interested in the subject.

Additional ways in which this work can be improved are listed below. The first three bullet points are contingent upon a successful development and incorporation of a computationally lighter reservoir response prediction model.

- **Allow switching between existing injectors and producers.** In this study, once the type of well was set between an injector and a producer, it was fixed for the remaining simulation run. A more realistic and versatile strategy will also involve switching a well between injectors and producers to maximize recovery.
- **Variable injection rates.** Injection rates for all injectors were fixed. This is an operational parameter that is highly adjustable. Injectivity at different wells may be variable; granting more flexibility in the injection rates may yield a more adaptive and feasible solution.
- **Stochasticity in the reservoir model.** Reduced computational overhead resulting from using a simple model will allow multiple reservoir

realizations, which can be used to reflect the uncertainty associated with the representation of the reservoir.

- **Adaptive exploration constant as the simulation progresses.** Because the NPV values calculated at time windows of the same width decrease as the recovery proceeds, by equation 4.2.1 on page 92, the relative contribution of the uncertainty increases, favoring exploration over exploitation. While this did not seem to drastically change the results, for scenarios where the NPV (or any measure of optimality) undergoes more change over time, such adaptive adjustment of the exploration constant may yield more reliable results.

- **Combine with the traveling salesman problem.** Although this study ignored the efficiency associated with the proximity of infill locations to be drilled consecutively, there are unavoidable costs involved with the logistics of transporting drilling rigs. Considering that, for instance, the costs of transferring offshore rigs are significantly higher than those of onshore rigs, including transport factor in the analysis may significantly help improve returns on investment.

Chapter 5

Conclusions

This concludes the discussion of the three decisional challenges solved in this dissertation. The solution to the water injection scheme optimization problem involved taking advantage of simple models (CRM and Koval's K-Factor method) and statistical methods (time series bootstrapping, EnOpt, and Thompson Sampling) to converge to a set of actions that are the most likely to be optimal. The computational workload were effectively reduced by focusing primarily on the forward simulations of decisions that were promising. A validation using a simulator is provided at the end of the chapter to demonstrate that the final selected water injection scheme is the most optimal among the ones generated by bootstrapping & EnOpt.

In the refrac timing problem, a real options method to generate an accurate estimate of the value of the refrac-candidate horizontal well. The LSM algorithm also provided with the policy that instructs the manager on when he should refrac the well depending on the gas prices and the gas production rates. Then the real options estimate of the value is compared against a more myopic, Monte Carlo discounted cash flow (MC-DCF) method to show that the latter provides an underestimate of the value because it fails to account

for the managerial flexibility inherent in the project.

Finally, in the infill drilling scheduling problem, the Monte Carlo tree search (MCTS) algorithm is used to find the optimal scheduling solution without suffering the curse of dimensionality. By pairing MCTS with a reservoir simulation model, we determined the optimal combination of wells, their configuration, and the order in which they should be drilled to maximize the returns on investment. A provisional validation is provided to compare the cumulative oil production and the NPV of the MCTS-optimized schedule against those resulting from randomly generated schedules.

Appendix: Approximating CRM for Infill Well Simulations

This section of the dissertation will outline an attempt to predict the production response of an undrilled location without relying on discretized reservoir simulators.

As described in section 2.2.1, CRM is a physically-derived model that takes on a data-driven approach in practical applications. In other words, while the CRM model is derived from a mass balance, the model is put to use by using nonlinear regression to fit the model parameters to historical production and bottomhole pressure data. The model is attractive because its parameters have physical relevance that are intuitive. However, the model cannot be immediately applied to determine the optimal infill drilling schedule because the candidate infill well locations do not have explicit injection or production data available for the model to capture well interactions.

The procedure discussed below is a workaround to this limitation to reduce the total amount of computation in optimal infill well scheduling. The objective is to develop an alternative representation of the reservoir that will accurately predict production responses at undrilled locations by modifying the CRM. The approach is as follows:

1. Using a reservoir simulator, drill all the candidate infill well locations.

2. Run the simulation using random, non-zero injection rates with perturbations.

3. Fit the CRM parameters using the generated production and flowing bottomhole pressure data.

4. Using the fitted CRM parameters from Step 3 and the porosity and permeability fields, determine the CRM parameters for cases where the infill wells are not drilled.

Despite that the first step relies on a reservoir simulator, the procedure will significantly reduce the amount of computations required overall if the generated model were to be used for the objective. This approach to proxy designing involves the following important assumptions:

- The CRM parameters are temporally stationary.
- The CRM parameters are independent of injection schemes (assuming non-zero, perturbed injections).
- The changes in CRM parameters resulting from removing a well can be accurately approximated using the CRM parameters pre-removal and simple geometric relations (except in limiting cases of extreme heterogeneity).

It is important to note that the four-step strategy described above takes the approach of beginning with the most number of wells and attempting to find the CRM parameters of the subset combinations of wells. This is because CRM parameters are, as discussed in section 2.2.1, summaries of distinct features of the inter-well system undergoing waterflooding. The time constants represent the rate at which producers respond to injection perturbations, the well connectivities indicate the relative contribution of injections from different injectors, and the productivity indices suggest the producer's responsiveness to local pressure drawdowns.

The fourth step in the method proposed above can potentially be achieved in multiple ways. Below lists approaches that remain to be explored in this work:

- Machine learning approach. Using multiple different realizations of well configurations in a reservoir simulation model, generate enough data to train the model to predict CRM parameters in undrilled locations. Consider random forest, gradient boosting machine (GBM), or XGBoost algorithms. An alternative to this would be to train the models to predict the rates directly.

- Time-of-flight- or streamline-based estimation. Generate a steady-state pressure solution, calculate time of flight for each cell, integrate time of

flight values along each streamline, and compare those results with CRM gains, time constants, etc.

- Start with a simple homogeneous reservoir, and mathematically/geometrically determine the CRM parameters at each point.

Bibliography

Beckner, B. L. and X. Song (1995). Field Development Planning Using Simulated Annealing-Optimal Economic Well Scheduling and Placement Optimal field-scale production of hydrocarbons must consider many reservoir, operational, and economic inputs and constraints. These inputs and constraints. Society of Petroleum Engineers.

Begg, S. H., R. Bratvold, and J. Campbell (2004). Abandonment Decisions and the Value of Flexibility. In *SPE Annual Technical Conference and Exhibition*, Houston, Texas, pp. 26–29.

Begg, S. H. and N. Smit (2007). Sensitivity of Project Economics to Uncertainty in Type and Parameters of Oil Price Models. In *SPE ATCE*, Anaheim, California. SPE International.

Brandão, L. E., J. S. Dyer, and W. J. Hahn (2005). Using Binomial Decision Trees to Solve Real-Option Valuation Problems. *Decision Analysis 2*(2), 69–88.

Bratvold, R. B. and S. H. Begg (2010). *Making Good Decisions*. Society of Petroleum Engineers.

Buckley, S. E. and M. C. Leverett (1941). Mechanism of Fluid Displacement in Sands. *Transactions of the AIME* (146), 107–116.

Carlstein, E. (1985). The Use of Subseries Values for Estimating the Variance of a General Statistic from a Stationary Sequence. *The Annals of Statistics 14*(3), 1171–1179.

Chen, Y. and D. Zhang (2009). Efficient Ensemble-Based Closed-Loop Production Optimization. *SPE Journal*.

Chitsiripanich, S. (2015). Field Application of CRM to Identify Potential Location for Infill Drilling. Master's thesis, The University of Texas at Austin.

Dixit, R. and R. Pindyck (2012). *Investment Under Uncertainty* (2nd ed.). Princeton University Press.

Efron, B. (1977). Bootstrap Methods: Another Look at the Jackknife. *The Annals of Statistics 7*(1), 1–26.

Friedman, J., T. Hastie, and R. Tibshirani (2009). *The Elements of Statistical Learning*.

Gentil, P. H. (2005). *The Use of Multilinear Regression Models in Patterened Waterfloods: Physical Meaning of the Regression Coefficients*. Ph. D. thesis, The University of Texas at Austin.

Gibson, R. and E. S. Schwartz (1990). Stochastic Convenience Yield and the Pricing of Oil Contingent Claims. *45*(3), 959–976.

Hall, P., J. L. Horowitz, and B.-Y. Jing (1995). On Blocking Rules for the Bootstrap with Dependent Data. *Biometrika 82*(3), 561–574.

Harvey, A. C. and S. Peters (1990). Estimation Procedures for Structural Time Series Models. Technical report.

Hong, A., R. B. Bratvold, and L. Lake (2018). Fast Analysis of Optimal IOR Switch Time Using a Two-Factor Production Model and Least-Squares Monte Carlo Algorithm. In *the SPE Norway One Day Seminar*.

Hong, A. J., R. B. Bratvold, and G. Naevdal (2016). Robust Production Optimization with Capacitance-Resistance Model as Precursor. *European Conference on the Mathematics of Oil Recovery* (September 2016).

Jansen, J. and R. Fonseca (2013). Improving the Ensemble Optimization Method Through Covariance Matrix Adaptation (CMA-EnOpt). *SPE Reservoir Simulation Symposium* (2006), 1–10.

Koval, E. J. (1963). A Method for Predicting the Performance of Unstable Miscible Displacement in Heterogeneous Media. *SPE J. 3*(2), 145–154.

Lake, L. W., R. Johns, B. Rossen, and G. Pope (2014). *Fundamentals of Enhanced Oil Recovery*. Society of Petroleum Engineers.

Liang, X., D. Weber, T. F. Edgar, L. W. Lake, M. Sayarpour, and A. Al-Yousef (2007). Optimization Of Oil Production Based On A Capacitance Model Of Production And Injection Rates. *SPE Hydrocarbon Economics and Evaluation Symposium* (SPE 107713), 11.

Longstaff, F. A. and E. S. Schwartz (2001). Valuing American Options by Simulation: A Simple Least-Squares Approach. *The Review of Financial Studies 14*(1), 113–147.

Mandal, D., N. Nabilah, N. Ahmad, and Carigali Petronas (2007). New Injection-Allocation Tool Significantly Improves the Value of Water Injection in Large Clastic Reservoirs. In *SPE Middle East Oil & Gas Show and Conference*, Kingdom of Bahrain, pp. 5.

Parra-Sanchez, C. (2010). *A Life Cycle Optimization Approach to Hydrocarbon Recovery*. Ph. D. thesis, The University of Texas at Austin.

Powell, W. (2011). *Approximate Dynamic Programming: Solving the Curses of Dimensionality*. John Wiley & Sons.

Russo, D., B. Van Roy, A. Kazerouni, I. Osband, and Z. Wen (2017). A Tutorial on Thompson Sampling.

Sayarpour, M. (2008). *Development and Application of Capacitance-Resistive Models to Water/CO2 Floods*. Ph. D. thesis, The University of Texas at Austin.

Schwartz, E. and J. E. Smith (2000). Short-Term Variations and Long-Term Dynamics in Commodity Prices. *Management Science 46*(7), 893–911.

Smith, J. E. (2005). Alternative Approaches for Solving Real-Options Problems. *Decision Analysis 2*(2), 89–102.

Smith, J. E. and K. F. McCardle (1998). Valuing Oil Properties: Integrating Option Pricing and Decision Analysis Approaches. *Operations Research 46*(2), 198–218.

Tavallali, M. S., I. A. Karimi, K. M. Teo, D. Baxendale, and S. Ayatollahi (2013). Optimal producer well placement and production planning in an oil reservoir. *Computers and Chemical Engineering 55*, 109–125.

Tavassoli, Z., J. N. Carter, and P. R. King (2004). Errors in History Matching. *SPE Journal 9*(3), 352–361.

Thomas, P. and R. B. Bratvold (2015). A Real Options Approach to the Gas Blowdown Decision. In *SPE Annual Technical Conference and Exhibition*, Houston, pp. 20. SPE.

Thomas, P. and L. W. Lake (2017). Valuing Historical Data in Water Injection Optimization Using the Capacitance Resistance Model.

Thompson, W. R. (1983). On the Likelihood that One Unknown Probability Exceeds Another in View of the Evidence of Two Samples. *Oxford Journals 25*(3), 285–294.

Weber, D. (2009). *The Use of Capacitance-Resistance Models to Optimize Injection Allocation and Well Location in Water Floods*. Dissertation, The University of Texas at Austin.

West, M. and J. Harrison (1997). *Bayesian Forecasting and Dynamic Models*. Springer-Verlag New York.

Williger, B. J. A. and R. Bratvold (2009). Valuing Oil and Gas Options by Least-Squares Monte Carlo Simulation. *SPE Projects, Facilities & Construction 4*(04).